DEVELOPMENT OF A SHUNT ACTIVE POWER FILTER FOR HARMONIC REDUCTION USING SYNCHRONOUS REFERENCE FRAME WITH SPACE VECTOR PULSE WIDTH MODULATION

BY

Sijuwade Akanni AKINTADE

Department of Electrical Engineering, Faculty of Engineering Ahmadu Bello University, Zaria, Nigeria

MARCH, 2019

DEVELOPMENT OF A SHUNT ACTIVE POWER FILTER FOR HARMONIC REDUCTION USING SYNCHRONOUS REFERENCE FRAME WITH SPACE VECTOR PULSE WIDTH MODULATION

BY

AKINTADE Sijuwade Akanni

P14EGEE8042

A DISERTATION SUBMITTED TO THE SCHOOL OF POSTGRADUATE STUDIES,

AHMADU BELLO UNIVERSITY, ZARIA

NIGERIA

IN PARTIAL FULFILMENT OF THE REQUIREMENTS FOR THE AWARD OF A MASTER OF SCIENCE (M.Sc) DEGREE IN ELECTRIC MACHINES AND INDUSTRIAL DRIVES

MARCH, 2019

DECLARATION

I, AKINTADE Sijuwade Akanni, hereby declare that the work in this dissertation entitled **"Development of a Shunt Active Power Filter for Harmonic Reduction Using Synchronous Reference Frame with Space Vector Pulse Width Modulation"** has been carried out by me in the Department of Electrical Engineering. The information derived from literature has been duly acknowledged in the text and a list of references provided. No part of this dissertation was previously presented for another degree or diploma at this or any other institution.

Akintade Sijuwade Akanni _____ _____

Signature Date

CERTIFICATION

This Dissertation entitled **"DEVELOPMENT OF A SHUNT ACTIVE POWER FILTER FOR HARMONIC REDUCTION USING SYNCHRONOUS REFERENCE FRAME WITH SPACE VECTOR PULSE WIDTH MODULATION"** by Sijuwade Akanni AKINTADE meets the regulations governing the award of degree of Master of Science (M.Sc) in Electric Machines and Industrial Drives of the Ahmadu Bello University, and is approved for its contribution to knowledge and literary presentation.

Dr. Y. Jibril Chairman, Supervisory Committee	_____ (Signature)	_____ Date
Prof. B. Jimoh Member, Supervisory Committee	_____ (Signature)	_____ Date
Dr. Y. Jibril Head of Department	_____ (Signature)	_____ Date
Prof. S.Z Abubakar Dean. School of Postgraduate Studies	_____ (Signature)	_____ Date

DEDICATION

This research work is dedicated to my lovely wife, glorious children, caring father and my late mother.

ACKNOWLEDGEMENT

I am grateful to Almighty God for sparing my life up to this moment and also given me the opportunity to carry out this wonderful research work. I wish to give my sincere thanks to my supervisor Dr. Y. Jibril for his valuable guidance and his unflinching support towards the success of this work. Thank you Sir. My appreciations also go to my co-supervisor Prof. B. Jimoh for his meticulous approach and always creating time for me in spite of his tight schedule. God bless you Sir. Many thanks to Dr. A.S Abubakar, for his valuable contributions. His criticisms, scrutiny and suggestions kept me going against all odds. Thank you Sir. My appreciation also goes to PG the coordinator Dr. G.A. Olarinoye for his contributions and support. May God reward him accordingly.

I acknowledge with thanks the entire teaching and non teaching staff of Electrical Engineering, Ahmadu Bello University, and most especially, those whose names could not be mentioned.

Finally, I would not have achieved any success without the support of my family; in this regards I would like to sincerely thank my parent, brothers, sisters, and my loving wife Oluwayomi for their patience, moral support, encouragement, and continual prayers. This equally goes to my children, Adetayo, Adedayo and Adeayo. I am grateful to you all for the perseverance, understanding and prayers. My profound gratitude equally goes to Ibrahim and my others course mate, friends and all well wishers. Thank you all for the support and cooperation rendered to me throughout this period.

Akintade Sijuwade Akanni

March, 2019

LIST OF ABBREVIATIONS

APF	–	Active Power Filter
IGBT	–	Insulated Gate Bipolar Transistor
IEEE	–	Institute of Electrical Engineers
IEC	–	International Electrotechnical Commission
IEEE	–	Institute of Electrical Engineers
LPF	–	Low Pass Filter
PCC	–	Point of Common Coupling
PI	–	Proportional Integral
PLL	–	Phase Lock Loop
PQ	–	Power Quality
PWM	–	Pulse Width Modulation
SPWM	–	Sinusoidal Pulse Width Modulation
SVPWM	–	Space Vector Pulse Width Modulation
THD	–	Total Harmonic Distortion
VSI	–	Voltage Source Inverter
SRF	–	Synchronous Reference Frame
FFT	–	Fast Fourier Transformation
THD	–	Total Harmonic Distortion
PI	–	Proportional Integral Controller
FLC	–	Fuzzy Logic Controller

ABSTRACT

This work aimed at designing and implementation of Shunt Active Power Filter (SAPF) for power quality improvement through harmonic reduction. The current harmonics are being caused by nonlinear characteristic of power electronics based equipments which increase power losses and in turn reduce power quality. This work employed a three phase three wire shunt active power filter implemented by simulation in MATLAB/Simulink for harmonic reduction. Synchronous Reference Frame (SRF) was used as a control strategy and for reference harmonic current generation and Space Vector Pulse Width Modulation (SVPWM) was adopted as current controller for switching signal generation of Voltage Source Inverter (VSI). With RL load under balanced voltage condition, the developed SAPF-SVPWM achieved a reduction of Total Harmonic Distortion (THD) of 0.91% as compared to 0.92% with Fuzzy Logic Pulse Width Modulation. In addition, the developed SAPF- SVPWM model was compared with SAPF without compensation using RL load under unbalanced voltage and the result shows that the developed SVPWM achieved reduction in THD from 26.68% to 1.74 % after and before compensation. All the results obtained are within IEEE 519 harmonics standard (i.e. THD less than 5%) with nonlinear load under balanced and unbalanced voltage. The result also shows an improvement of 1.087% with RL load under balanced voltage. This confirmed the effectiveness of the SAPF in harmonics reduction.

TABLE OF CONTENTS

TITLE PAGE

DECLARATION i

CERTIFICATION ii

DEDICATION iii

ACKNOWLEDGEMENT iv

ABBREVIATIONS v

ABSTRACT vi

TABLE OF CONTENTS vii

LIST OF FIGURES ix

LIST OF TABLES xiv

LIST OF APPENDICES xiv

LIST OF SYMBOLS xv

CHAPTER ONE: INTRODUCTION

1.1 Background 1

1.2 Significance of Research 3

1.3 Statement of Problem 3

1.4 Aim and Objectives 4

CHAPTER TWO: LITERATURE REVIEW

2.1 Introduction 6

2.2 Review of Fundamental Concepts 6

2.2.1 Power Quality 6

2.2.2 Waveform Distortion 11

2.2.3 Filters 15

2.2.4 Shunt Active Power Filter Parameters Design Approach 21

2.2.5 Harmonics Current Extraction Strategies 24

2.2.6 Control Strategies in SAPF 25

2.3 Review of Similar Works 34

CHAPTER THREE: METHODOLOGY

3.1 Introduction 41

3.2 Methodology 41

3.3 Selection of Shunt Active Power Filter Design Parameters 42

3.3.1 Selection of DC Reference Voltage 43

3.3.2 Selection of Coupling Inductor 43

3.3.3 Selection of DC Side Capacitor 43

3.4 Modeling of Shunt Active Power Filter in d-q 44

3.4.1 Control in Synchronous Frame Reference (d-q) 47

3.4.2 DC Bus Control Using PI 48

3.5 Design of Space Vector Pulse Width Modulation (SVPWM) 50

3.5.1 Determination of V_d , V_q , V_{ref} and Angle α 50

3.5.2 Determination of Time Duration T_0 , T_1 and T_2 52

3.5.3 Determination of Switching Time of Each Transistor 55

CHAPTER FOUR: RESULTS AND DISCUSSION

4.1 Introduction 59

4.2 Output Waveform of SVPWM with SAPF 59

4.3 SAPF with Balanced Voltage 60

4.3.1 Waveform of RL Load before Compensation 60

4.3.2 Waveform of RL Load after Compensation with SVPWM 61

4.3.3 Result of FFT Analysis of RL Load before Compensation 62

4.3.4 Result of FFT Analysis of RL Load after Compensation with SVPWM 62

4.3.5 Waveform of RC Load before Compensation 64

4.3.6 Waveform of RC Load after Compensation with SVPWM 64

4.3.7 Result of FFT Analysis of RC Load before Compensation 66

4.3.8 Result of FFT Analysis of RC Load after Compensation with SVPWM 66

4.4 SAPF with Unbalanced Voltage 68

4.4.1 Waveform of RL load before compensation 68

4.4.2 Waveform of RL Load after Compensation with SVPWM 69

4.4.3 Result of FFT Analysis of RL Load before Compensation 70

4.4.4 Result of FFT Analysis of RL Load after Compensation with SVPWM 70

4.4.5 Waveform of RC Load before Compensation 72

4.4.6 Waveform of RC Load after Compensation with SVPWM 72

4.4.7 Result of FFT Analysis of RC Load before Compensation 74

4.4.8 Result of FFT Analysis of RC Load after Compensation with SVPWM 74

CHAPTER FIVE: CONCLUSION AND RECOMMENDATION

5.1 Conclusion 76

5.2 Limitation 76

5.3 Significant Contributions 76

5.4 Recommendations 77

REFERENCES 78

LIST OF FIGURES

Figure 2.1: Over voltage Waveform 7

Figure 2.2: Under voltage Waveform 7

Figure 2.3: Voltage interruption Waveform 8

Figure 2.4: Voltage fluctuations waveform 9

Figure 2.5: Unbalanced in Three Phase System Waveform 9

Figure 2.6: Voltage waveform during voltage sag 9

Figure 2.7: Voltage Spike Waveform 10

Figure 2.8: Voltage swell waveform 10

Figure 2.9: Harmonic waveform 11

Figure 2.10: Passive Shunt Filter Block Diagram 16

Figure 2.11: Series Active Power Filter Diagram 17

Figure 2.12: Hybrid Active Power Filter Diagram 18

Figure 2.13: Basic Configuration of a SAPF Block Diagram 19

Figure 2.14: Shunt Active Filter Block Diagram 20

Figure 2.15: Compensating Power Exchange between the Grid and Shunt APF 21

Figure 2.16: Triangular Carrier Pulse Width Modulation Waveform 27

Figure 2.17: Space Vector Representation Diagram 29

Figure 2.18: Three Phase Inverter Block Diagram 30

Figure 2.19: Switching Configuration of a Three-Phase Inverter 30

Figure 2.20: Space Vectors of Three-Phase Bridge Diagram 31

Figure 3.1: A 3-ph, 3-wire SAPF connected to the grid and load at PCC 42

Figure 3.2: Block Diagram of Principle of the Synchronous Reference Method 45

Figure 3.3: Direct Control by PI Controllers in the Synchronous Reference 47

Figure 3.4: Current Controllers in Synchronous Reference Block Diagram 48

Figure 3.5: DC Voltage Control Loop Block Diagram 49

Figure 3.6: Voltage Space Vector and its Components in (D- Q) 51

Figure 3.7: Reference Vector as a Combination of Adjacent Vectors at Sector 1 52

Figure 3.8: Space Vector PWM Switching Patterns at each Sector 55

Figure 3.9 Flow chart for SVPWM implementation 57

Figure 3.10 SVPWM based current control scheme for generating switching pulses 58

Figure 4.1: Output Switching Pulse of SVPWM at 20 KHz 59

Figure 4.2: Waveforms of RL Load: Source Voltage (Vs), Source Current before Compensation 60

Figure 4.3: Simulation Waveform of RL Load with SVPWM: Source Voltage (Vs), Source Current (Is) after Compensation, Compensation Current (Ic) and DC Bus Voltage (V_{dc}). 61

Figure 4.4: FFT Analysis of Source Current (Is) with RL Load before Compensation 62

Figure 4.5: FFT Analysis of the Source Current (Is) after Compensation with SVPWM for RL Load 63

Figure 4.6: Waveforms of RC Load: Source Voltage (Vs), Source Current before Compensation 64

Figure 4.7: Simulation Waveform of RC Load with SVPWM: Source Voltage (Vs), Source Current (Is) after Compensation, Compensation Current (Ic) and DC Bus Voltage (V_{dc}). 65

Figure 4.8: Waveforms of RC Load: Source Voltage (Vs), Source Current before Compensation 66

Figure 4.9: FFT Analysis of the Source Current (Is) after Compensation with SVPWM for RC Load 67
Figure 4.10: Waveforms of RL Load under Unbalanced Voltage: Source Voltage (Vs), Source Current before Compensation 68
Figure 4.11: Simulation Waveform of RL Load with SVPWM Under Unbalanced Voltage: Source Voltage (Vs), Source Current (Is) after Compensation, Compensation Current (Ic) and DC Bus Voltage (V_{dc}). 69
Figure 4.12: FFT Analysis of the Source Current (Is) before Compensation with SVPWM for RL Load Unbalanced Voltage 70
Figure 4.13: FFT Analysis of the Source Current (Is) after Compensation with SVPWM for RL Load under Unbalanced Voltage 71
Figure 4.14: Waveforms of RC Load under Unbalanced Voltage: Source Voltage (Vs), Source Current before Compensation 72
Figure 4.15: Simulation Waveform of RC Load with SVPWM under Unbalanced Voltage: Source Voltage (Vs), Source Current (Is) after Compensation, Compensation Current (Ic) and DC Bus Voltage (V_{dc}). 73
Figure 4.16: FFT Analysis of the Source Current (Is) before Compensation with SVPWM for RC Load under Unbalanced Voltage 74
Figure 4.17: FFT Analysis of the Source Current (Is) after Compensation with SVPWM for RC Load under Unbalanced Voltage 75

LIST OF TABLES

Table 2.1 Space Vectors, Switching States, and On State Switches 32

Table 2.2: Parameters of the a Switching Vectors, Phase Voltages and Output Line to Line Voltages 33

Table 3.1: SAPF Parameters (Suleiman *et al.*, 2017) for Balanced Voltage 43

Table 3.2: Switching Time Calculation at Each Sector 56

Table 4.1: Summary of Results of Balanced Voltage System with SAPF 67

Table 4.2: Summary of Results of RL Non Linear Load with Unbalanced Voltage System with SAPF 75

LIST OF APPENDICES

APPENDIX A 83

Simulink Models of SAPF 83

Simulink Models of SVPWM 83

LIST OF SYMBOLS

C_{dc}	DC link capacitor
M_a	Amplitude modulation ratio
V_{dc}	dc link voltage
V_{dcref}	Reference dc link voltage
ω	Angular frequency of the output voltage
L_f	Shunt interfacing inductor
θ	Grid impedance angle
f	Fundamental frequency
V_f	Inverter output voltage
I_s	Source current
I_f	Shunt active filter compensation current
I_d , I_q	Currents in synchronous reference frame
I_α , I_β	Currents in the α-β frame
U_α, U_β	Voltages in the α-β frame
V_d, V_q	Voltages in the d-q frame

CHAPTER ONE

INTRODUCTION

1.1 Background

Power quality is greatly influenced by nonlinear loads such as power electronics equipment, electrical drives, compact fluorescent lamp, oven among others which inject harmonics into distribution system (Abhijit & Kompelli, 2016; Chennia & Benchouia, 2011; Soomro *et al.*, 2015: Umar, 2017). Therefore, as electric power is generated, distributed and utilized, voltage and current waveforms distortions are produced. These distortions are known as harmonics, and thereby cause changes in the electrical nature of the current and voltage of the power supply. Harmonics degrade power quality by increasing Total Harmonic Distortion (THD) and reactive power consumption lead to poor power factor, voltage flicker, bad voltage regulation, voltage sags and swells (Suresh & Anup, 2011; Suleiman *et al.*, 2017; Akash *et al.*, 2016). It also leads to significant economic losses due to fact that some electrical equipments are sensitive to power quality problem (Suleiman *et al.*, 2017).

Passive power filter is a traditional restraint harmonic mitigation method; because it is limited in its ability to reduce harmonic current in the distribution system. Passive power filter also suffers many drawbacks such as heavy weight and bulky sizes, series and parallel resonance with system impedance (Abhijit & Kompelli, 2016; Chennia & Benchouia, 2011; Sindhu *et al.*, 2015; Suleiman *et al.*, 2017; Varaprasad & Siva, 2014; Naresh & Prabhat, 2012). Passive filter (combination of capacitor and inductor) were used to mitigate the Power Quality (PQ) problems. This approach was extensively used in High Voltage Direct Current transmission (HVDC) for

filtering the harmonics on AC and DC sides. However, this approach is not suitable at the distribution level as passive filter can only correct specific load condition (Soomro *et al.,* 2015)

In recent times Active Power Filters (APF) were introduced and accepted as one of the most common compensation method. APF are switch mode power electronics converters that injects harmonics current in equal and opposite phase at point of common coupling (PCC) so that utility need to supply only the distortion free currents (Saravanan & Balachrishnan, 2014; Sindhu *et al.,* 2015; Akash *et al.,* 2016; Niklesh & Sandeep, 2017). There are three types of active power filter (APF) which are shunt, series and hybrid which is the combination of active and passive filter (Soomro *et al.,* 2015). The effectiveness of shunt active power filter (SAPF) depends on the methods used to obtain the reference current, current controller, power inverter topology and DC-link voltage (Venkata *et al.,* 2014; Chennia & Benchouia, 2014; Akash & Mukund, 2015; Ali *et al.,* 2015; Suleiman *et al.,* 2017).

There are many control scheme for reference current generation and harmonics extraction techniques that have been used for improving the steady state and dynamic performance of APF, such as synchronous reference frame (d-q-o) theory, instantaneous real-reactive power (p-q) theory, modified instantaneous (p-q) theory, flux-based controller, notch filter and Artificial Neural Network (ANN) techniques (Zahira & Peer, 2011; Narsesh & Prabhat, 2012; Chelli *et al.,* 2015). Instantaneous power theory is widely used in different research work; this technique provide good results under different voltage source conditions but present some drawbacks such as much calculation which necessitates complex mathematical transformation and difficult implementation in practice (Chennia & Benchouia, 2011; Chelli *et al.,* 2015). Synchronous Reference Frame (SRF) theory is commonly used in three phase system for reference current

generation from the load current and this due because of its simplicity, easy implementation, accuracy and dynamics response (Abhijit & Kompelli, 2016).

Similarly, various current control methods such as hysteresis, triangular wave control, dead beat control, Space vector pulse width modulation among others have been presented in the literature (Naresh & Prabhat, 2012). Space Vector Pulse Width Modulation (SVPWM) is a more sophisticated, advanced, computation intensive technique for generating sine wave that provides a higher voltage with lower total harmonic distortion and is one of the best among all the pulse width modulation techniques because of advantages of low switching loss, wide range of modulation index and less harmonics distortion. SVPWM technique also utilizes the DC bus voltage more efficiently when compared with the other techniques (Phuong 2012).

1.2 Significance of Research

The significance of this research is the development of a shunt active power filter based SVPWM techniques for switching pulse generation to mitigate the load current harmonic cause by non linear loads under balanced and unbalanced input voltage condition.

1.3 Problem Statement

Harmonic generation is undesirable outcome of industrial electronic devices and non-linear loads. The harmonics in the system induce several undesirable issues; such as increased heating in transformers, low power factor, and voltage drop across the network impedance (Akash *et al.*, 2016).

Shunt active power filter has proven to be the best for both harmonics current and reactive-power compensation. Shunt active power line conditioner is most commonly used among the topologies of active power filter. The effectiveness of shunt active power filter depends on the methods used

to obtain the reference current. Several methods of harmonics current identification and extraction techniques such as synchronous reference frame (d-q), instantaneous real-reactive power (p-q) and synchronous detection method have been used (Chelli, *et al.,* 2015). SRF technique is chosen because of simplicity and easy implementation. Generation of compensation current by SAPF depends also on switching strategy used. The hysteresis, SPWM and artificial intelligent current control techniques are generally used by many researchers (Naresh & Prabhat, 2012). The drawback of fuzzy logic is the over dependent on expert rules and large number of membership function for it effective performance and this drawbacks make fuzzy logic difficult or almost impossible to achieve. In this work, SVPWM is used to improve the performance of SAPF because of the advantages of low switching loss, wide range of modulation index and less harmonics distortion.

1.4 Aim and Objectives

The aim of the research is to design shunt active power filter for harmonic reduction using synchronous reference frame with space vector pulse width modulation.

The objectives of the research are as follows:

1. Development of Shunt Active Filter (SAPF) parameters. Adopted from the work of Suleiman *et al.,* (2017).
2. Development of a control strategy model for Shunt Active Power Filter (SAPF) for the extraction of reference harmonic current.
3. Implementation of a current controller technique for switching pulse generation for voltage source inverter using MATLAB/SIMULINK.

4. Validation of the developed SAPF performance under balanced and unbalanced sinusoidal voltage conditions using IEEE 519 harmonic standard (That is THD less than 5%) and the work of Suleiman *et al.*, 2017.

CHAPTER TWO

LITERATURE REVIEW

2.1 Introduction

This chapter presents details of overview of fundamental concept and the review of similar works.

2.2 Review of Fundamental Concept

Fundamental Concepts of this research work are reviewed in this section.

2.2.1 Power Quality

The term power quality is defined as properties of power quality as supply to user in common operating condition in term of continuity of power supply and feature of voltage like symmetry, frequency, magnitude and waveform as described in IEC and according to IEEE standard (Mohammed, 2012). The increasing use of power semiconductors in the most of industrial and domestic procedures, the electric grids are polluted with different harmonic currents and voltages (Mohammed, 2012). Power quality include all the concerned sides of power supply, which are under voltage, over voltage, voltage sag, voltage swell, phase shift, flicker, frequency, transient, voltage unbalanced e.t.c. (Yogesh, 2014; Mohammed, 2012; Hussein, 2012). The maximum tolerable value of harmonics pollution in term of THD should be less than 5% according to IEEE-519 standard.

2.2.1.1 Over voltage

It is a momentary increase in voltage outside the normal tolerance most especially when the voltage variations exceed 110 percent of the terminal value. The diagram of over voltage is shown in Figure 2.1. Faults and switching off of heavy electrical equipment cause voltage swell. The increased energy from a voltage swell often overheats equipment and reduces its life.

Voltage regulator, motor-generator set and uninterruptible power supply can mitigate the voltage swell effects (Hussein, 2012).

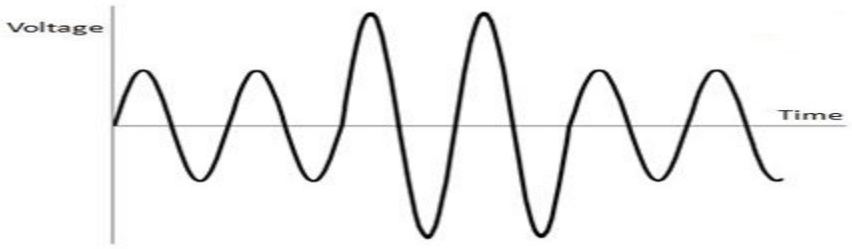


Figure 2.1: Over Voltage Waveform (Hussein, 2012)

2.2.1.2 Under voltage

It is a decrease in the root mean square (rms) ac voltage to less than 90% of the nominal value as shown Figure 2.2. A load switching on or a capacitor bank switching off can cause an under voltage until the voltage regulation equipment in the system brings the voltage back within tolerances. Overloaded circuits and the loss of major transmission support can also result in under voltages. It can cause sensitive computer equipment to read data incorrectly and motor to stall and operate inefficiently (Hussein, 2012).

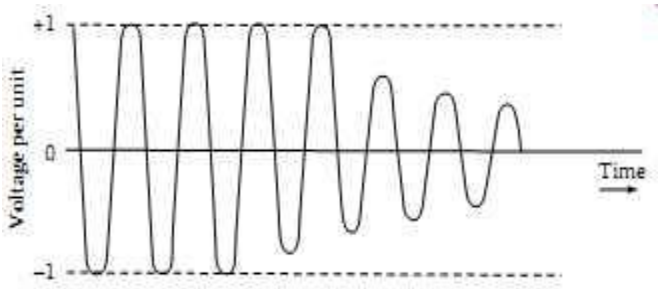


Figure 2.2: Under Voltage Waveform (Hussein, 2012)

2.2.1.3 Voltage Interruption

The cutoff of the voltage happens when the load voltage decreases until less than 10% of its nominal value for a short period of time less than 1 minute as shown in Figure 2.3. The voltage interruption can be the effect of defaults in the electrical system, defaults in the connected

equipments, or bad control systems. The main characteristic of the voltage interruption is the period over which it happens (Mohammed, 2012).

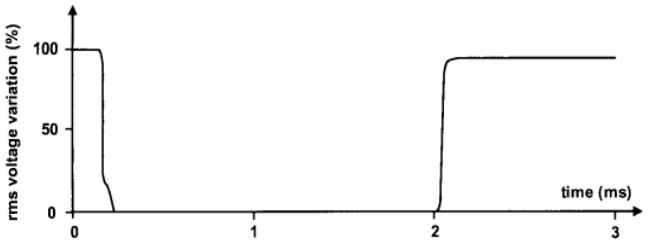


Figure 2.3: Voltage Interruption Waveform (Emmanuel, 2012)

2.2.1.4 Voltage Fluctuations (Flicker)

They are cyclical variations in the voltage root mean square (rms) values or a series of random voltage changes, whose magnitude does not normally exceed voltage ranges of 0.9 p.u. to 1.1 p.u (Hussein, 2012) as shown in Figure 2.4. A common phenomenon of voltage fluctuations is the voltage flicker. Loads, which can exhibit continuous, rapid variations in the load current magnitude can cause voltage fluctuations or flickers (Hussein, 2012).

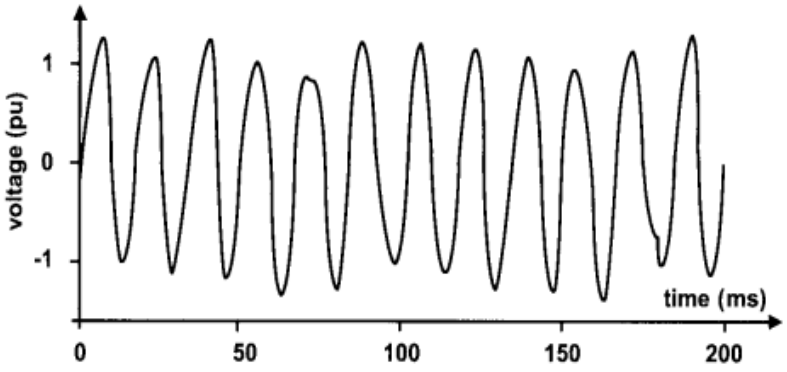


Figure 2.4: Voltage Fluctuations Waveform (Emmanuel, 2012)

2.2.1.5 Unbalanced in Three Phase Systems

The three phase system is unbalanced when the currents and voltages are not identical in amplitude; or when the phase angle between each two phases is not 120^0 as shown in Figure 2.5. In the ideal conditions, the three phase system is balanced with identical loads but in reality, the

loads are not identical (Mohammed, 2012). The ratio of either the negative or zero sequence components to the positive sequence component can be used to specify the percent imbalance (Hussein, 2012).

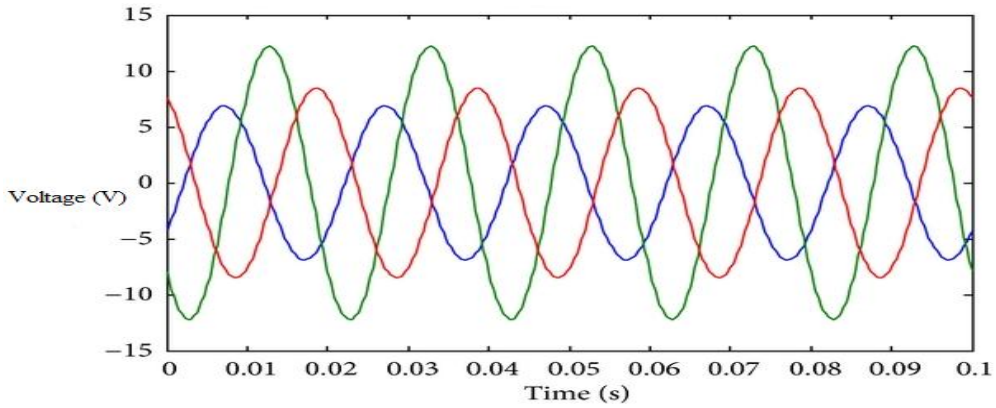


Figure 2.5: Unbalanced in Three Phase System (Ravindra *et al.*, 2012)

2.2.1.6 Voltage Dips

The voltage dips or sags are periodic perturbations. This phenomenon causes bad functioning of the protection equipments (Mohammed, 2012). It is a reduction in voltage outside the normal tolerance for a short time less than few seconds. The magnitude of the reduction is between 10 percent and 90 percent of the normal (rms) voltage as shown in Figure 2.6 (Hussein, 2012).

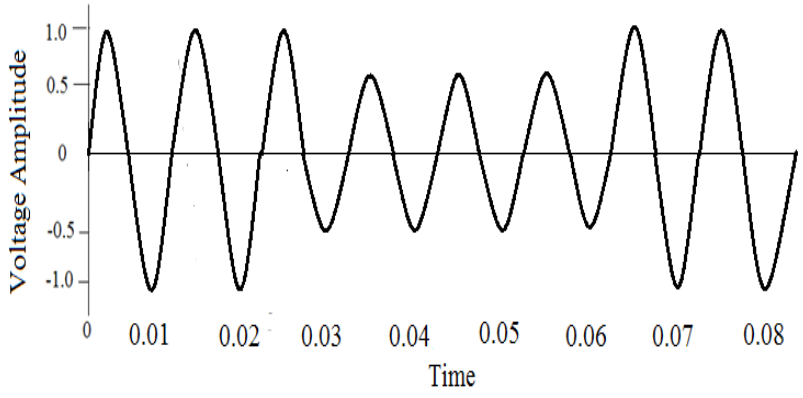


Figure 2.6: Voltage Waveform during Voltage Sag (Hussein, 2012)

2.2.1.7 Voltage Spikes and Surges

It is a short duration from microsecond to millisecond voltage increase as shown in Figure 2.7. It occurs due to lightning, switching of heavy loads and power system faults. It leads to equipment failure, system lock-up, data corruption and data loss. Solutions to voltage spikes and surges problems include equipment such as surge arresters, filters and isolation transformer (Hussein, 2012).

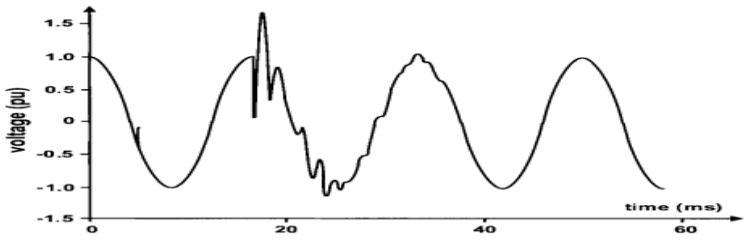


Figure 2.7: Voltage Spike Waveform (Emmanuel, 2012)

2.2.1.8 Voltage Swell

It is a momentary increase in voltage outside the normal tolerance as shown in Figure 2.8. Faults and turning off of heavy electrical equipment cause voltage swell. The increased energy from a voltage swell often overheats equipment and reduces its life. Voltage regulator, motor-generator set and uninterruptible power supply can mitigate the voltages swell effects (Hussein, 2012).

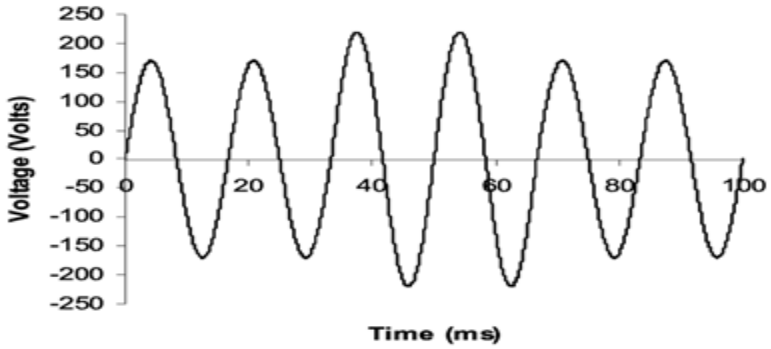


Figure 2.8: Voltage Swell Waveform (Hussein, 2012)

2.2.2. Waveform Distortion

Waveform distortion is defined as a steady-state deviation from an ideal sinusoidal wave of power frequency. It is characterized by the spectral content of the deviation (Karuppananp, 2012). Primary types of waveform distortion are harmonics, notching, inter-harmonics, DC offset and noise (Karuppananp, 2012).

2.2.2.1 Harmonics

Harmonic related problems are not new in the electric power system. From the early 1920's harmonics are observed in power equipment because of telephone line interference. The proliferation of power converter equipment connected to the distribution power system which limits harmonic current injection maintains good power quality (Karuppanan, 2012).

Harmonics are sinusoidal voltages or currents having frequencies that are integer multiples of the fundamental frequency (Hussien, 2012). Distorted waveforms can be decomposed into the sum of the fundamental frequency and the harmonic components as shown in Figure 2.9.

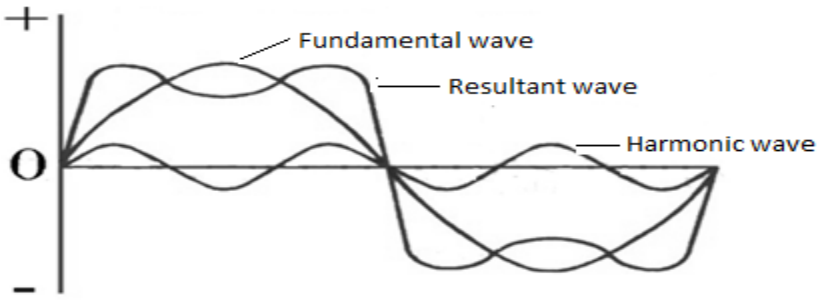


Figure 2.9: Harmonic Waveform (Hussein, 2012)

The following are the effect of harmonics (Karuppananp, 2012)

i. Amplification of harmonic levels resulting from series and parallel resonance.

ii. Plant mal-operation.

iii. Malfunctioning and failure of electronic components.

iv. Overheating and failure of electric motors.

v. Overloading, overheating and failure of power factor correction capacitors.

vi. Overloading % errors in metering equipments.

vii. Spurious operation of fuses, circuit breakers and other protective equipments.

viii. Voltage glitches in computer systems results in loss of data.

ix. Electromagnetic interference in HF communication systems such as television, radio, communication and telephone systems and similar signal conditioning devices.

Harmonics also have the following economic effect (Karuppanan, 2012).

i. Higher power cost

ii. Premature office equipment failure and data corruption or loss

iii. Computer and system lockups

iv. Loss of productivity and higher cost of products and/or services

v. Reduced product or service quality and reduced quality assurance

vi. Loss of customer confidence and revenue

There are two types of harmonics that can be encountered in a power system which are synchronous harmonics and asynchronous harmonics. Synchronous harmonics are sinusoids with frequencies which are multiples of the fundamental frequency. The synchronous harmonics can be subdivided into two categories (Mohammed, 2012).

i. Sub-harmonics: when the harmonic frequency is less than the fundamental frequency.

ii. Super harmonics: when the harmonic frequency is more than the fundamental frequency.

The rapid growth of solid-state power electronics has greatly increased the number and size of these loads. The concept of harmonics was introduced in the beginning of the 19th century by Joseph Fourier. Fourier has demonstrated that all periodic non-sinusoidal signals can be

represented by infinitive sum or series of sinusoids with discontinuous frequencies (Mohammed, 2012). The distorted periodic current and voltage waveform expanded into a Fourier series is expressed as follows: (Hussein, 2012).

$$I(t) = I_0 + \sum_{h=1}^{\alpha} I_h \cos(h\omega t + \Phi_h) \quad (2.1)$$

$$V(t) = V_0 + \sum_{h=1}^{\alpha} V_h \cos(h\omega t + \Phi_h) \quad (2.2)$$

Where,

I_0 and V_0 are the direct component of current and voltage

I_h and V_h are the h^{th} harmonic peak current and voltage

Φ_h is the h^{th} harmonic current and voltage phase

ω is angular frequency

2.2.2.2 Total Harmonic Distortion (THD)

The total harmonic distortion (THD) of a signal is a measurement of the harmonic distortion present in current or voltage. It is defined as the ratio of the sum of the powers of all harmonic components to the fundamental component. Harmonic distortion is caused by the introduction of waveforms at frequencies in multiplies of the fundamental (Mohammed, 2012).

The most commonly used harmonics indexes are shown as follows: (Hussein, 2012).

$$THD_V(\%) = \frac{\sqrt{\sum_{h=2}^{\alpha} V_h^2}}{V_1} \quad (2.3)$$

$$THD_I(\%) = \frac{\sqrt{\sum_{h=2}^{\alpha} I_h^2}}{I_1} \quad (2.4)$$

Total Harmonic Distortion is defined as the ratio of the rms value of the harmonic components to the rms value of the fundamental component and usually expressed in percent. This index is used to measure the deviation of a periodic waveform containing harmonics from a perfect sine wave. For a perfect sine wave at fundamental frequency, the THD is zero.

Similarly, the measures of individual harmonic distortion for voltage and current at h^{th} order are defined as V_h / V_1 and I_h / I_1, respectively (Hussein, 2012).

The Total Harmonic Distortion (THD) is a useful tool for many applications, most especially in measurement of harmonic index. However, its limitation is that, it is not a good indicator of voltage stress within a capacitor because that is related to the peak value of voltage waveform (Mohammed, 2012).

2.2.2.3 Distortion Factor

The distortion factor (F_D) is defined as the ratio between the fundamental and the signal in root mean square (RMS) values. It is then equal to unity when the current is purely sinusoidal and decreases when the distortion appears (Mohammed, 2012). The distortion factor (F_D) equation can be obtained as follows: (Mohammed, 2012).

$$F_D = \frac{I_{L1}}{I_{rms}} \tag{2.5}$$

Where,

I_{L1} is the fundamental value of current

I_{rms} is the RMS value of current

2.2.2.4 Crest Factor

The crest factor (F_c) of a signal be obtained as the ratio of crest maximum value to effective value. The crest factor for sinusoidal waves is 1.41. It can achieve the value of 5 in the case of highly distorted waves. The crest factor (F_c) is expressed as follows: (Mohammed, 2012).

$$F_C = \frac{I_{max}}{I_{rms}} \tag{2.6}$$

Where,

I_{max} is the crest maximum value

I_{rms} is the rms value of current

2.2.3 Filters

There are three different types of filters each offering their own unique solution to reduce and eliminate harmonics. These harmonic filters are broadly classified into passive, active and hybrid structures. The choice of filter used is dependent upon the nature of the problem and the economic cost associated with implementation (Nalini *et al.,* 2011).

2.2.3.1 Passive Filter

It is a combination of inductors, capacitors, and resistors designed to eliminate one or more harmonics (Roger *et al.,* 2004). The most common type is simply an inductor in series with a shunt capacitor, which short-circuits the major distorting harmonic component from the system. Passive filters are inexpensive compared with most other mitigating devices. Its structure may be either of the series or parallel type. The structure chosen for implementation depends on the type of harmonic source present. There are many types of passive filters, the most common ones are single-tuned filters and high-pass filters. This type of filter removes the harmonics by providing

a very low impedance path to the ground for harmonic signals. Passive filters has disadvantages such as frequency variation of the power system, tolerances in filter components which affect the compensation characteristics of the LC filters and source impedance which influences the compensation characteristics of the LC filters (Nalini *et al.*, 2011; Roger *et al.*, 2004; Farzad & Mahid, 2014; Balasubramaniam *et al.*, 2014; Mohamed *et al.*, 2017). Conventionally, passive LC filters have been used to eliminate line current harmonics and thereby increase the load power factor. Passive filters can be classified into three categories such as passive shunt, passive series and passive hybrid. Passive shunt is the commonly used among the three classifications. Figure 2.10 shows the schematic diagram of passive shunt filter (Manjulata, 2012).

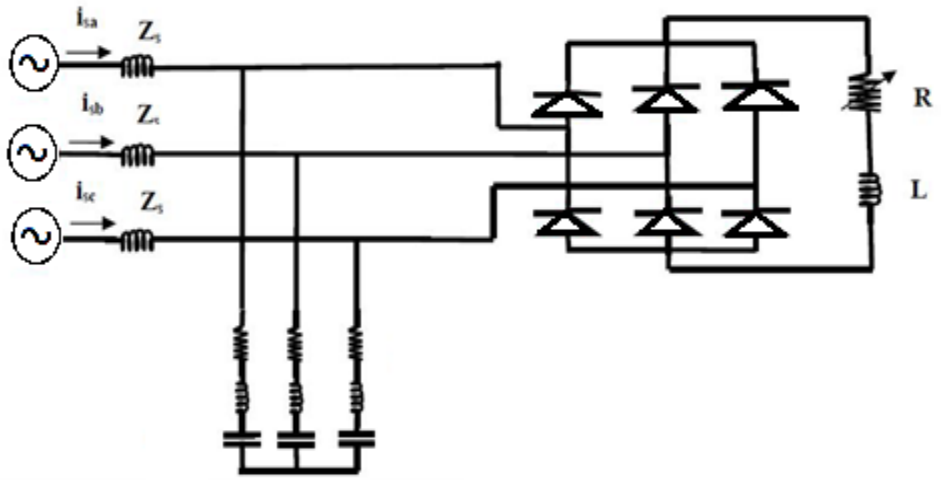


Figure 2.10: Passive Shunt Filter Block Diagram (Manjulata, 2012)

2.2.3.2 Active Filters

Active filters use active components such as IGBT transistors to inject negative harmonics into the network and effectively replacing a portion of the distorted current wave coming from the load (Nalini *et al.*, 2011). Active filter is implemented when orders of harmonic currents are varying. Its structure may be either of the series or parallel type and the structure is chosen based on the type of harmonic sources present in the power system and the effects that different filter

solutions would cause to the overall system performance (Nalini *et al.,* 2011). Active filters have the advantage of being able to compensate for harmonic without fundamental frequency reactive power concerns. Another advantage of active filters over passive filters is that the active filters can respond to changing load and harmonic conditions, whereas passive filters are fixed in their harmonic response. (Sankara, 2002; Nalini *et al.,* 2011).

Active filter can be classified based on the connection scheme as shunt active filter, Series active filter and Hybrid active filter. Hybrid filters combine an active filter and a passive filter. Its structure may be either of the series or parallel type. The passive filter carries out basic filtering (5th order, for example) and the active filter, through precise control, covers higher harmonics. Shunt active filter is most commonly used among the three classifications (Balasubramaniam *et al.,* 2014).

2.2.3.3 Series Active Power Filter

The aim of the series APF is to locally modify the impedance of the grid. It is considered as harmonic voltage source which cancel the voltage perturbations which come from the grid or these created by the circulation of the harmonic currents into the grid impedance as shown in Figure 2.11. However, series APFs can't compensate the harmonic currents produced by the loads (Mohammed, 2012).

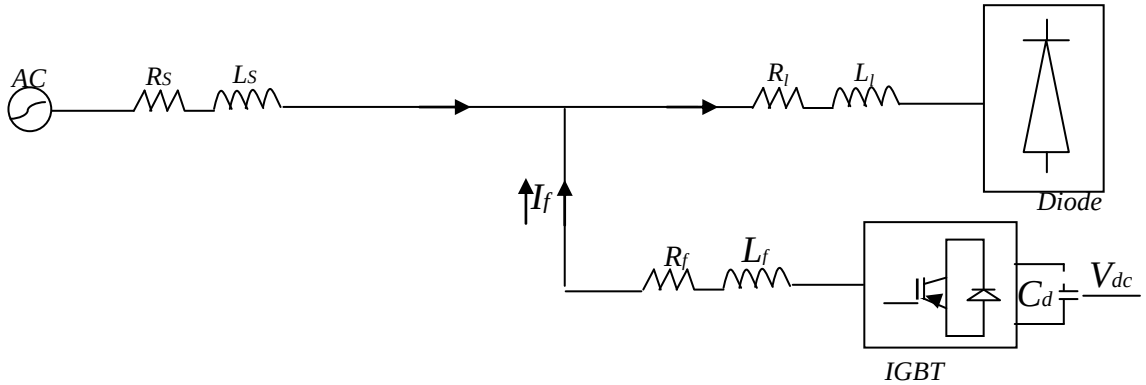


Figure 2.11: Series Active Power Filter Diagram (Mohammed, 2012)

2.2.3.4 Hybrid Filters

Hybrid filter is a filter topology which combines the advantages of the passive and active filters in other to mitigate the issues of active and passive filters as shown in Figure 2.12. It provides value effective and sensible harmonic compensation approach for prime power non linear loads Hemachandran *et al.*, 2015; Mohammed, 2012). The Volt Ampere rating of the active converter is reduced as much as possible in order to reduce the overall cost, electromagnetic interference and losses and this reason, it is considered as the best solution to eliminate the harmonic currents from the grid. Economically, hybrid power filters allow reducing the cost of implementation of APF (Naresh & Prabhat., 2012; Mohammed, 2012).

Hybrid power filters can be classified according to the number of elements used in the topology, the treated system (single phase, three phase three legs or four legs) and the used inverter type (current source inverter or voltage source inverter) (Mohammed, 2012).

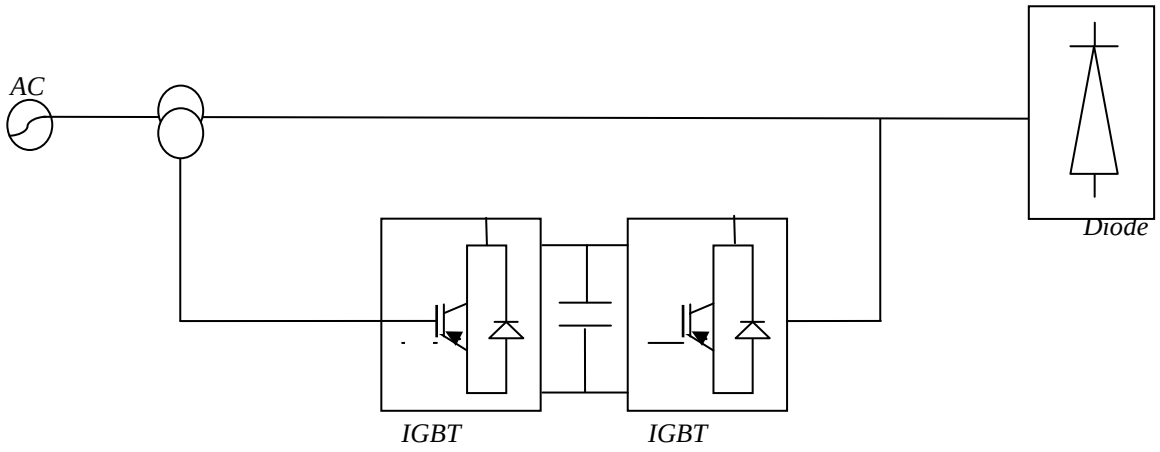


Figure 2.12: Hybrid Active Power Filter Diagram (Mohammed, 2012)

2.2.3.5 Shunt Active Power Filter (SAPF)

The active filter concept uses power electronic equipment to produce harmonic current components that cancel the harmonic current components from the nonlinear loads. In this configuration, the filter is connected in parallel with the load being compensated; therefore the configuration is often referred to as an active parallel or shunt filter (Nalini *et al.,* 2011). The basic principle of Shunt Active Filter is that it generates a current equal and opposite to the harmonic current drawn by the load and injects it to the point of coupling there by forcing the source current to be pure sinusoidal (Nalini *et al.,* 2011). The basic configuration of a shunt active filter is shown in Figures 2.13.

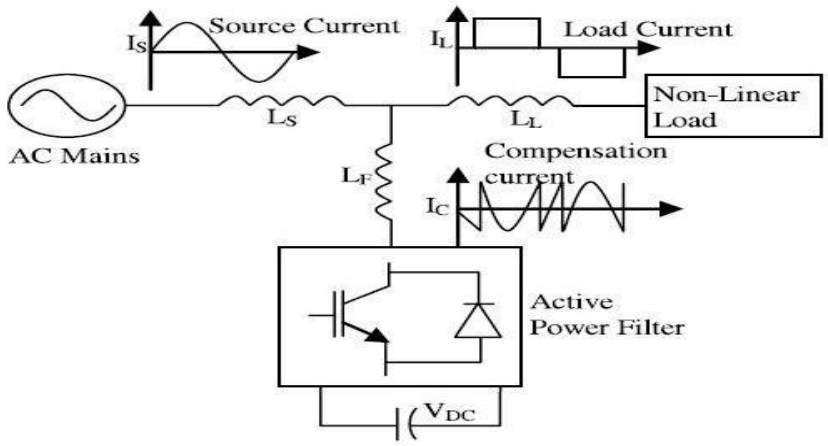


Figure 2.13: Basic Configuration of a SAPF Block Diagram (Abdeldjabbar & Tayeb, 2017)

The three-phase source voltages equation is given as (Suleiman *et al.,* 2017).

$$V_{sa} = V_{sm}\sin(wt)$$
$$V_{sb} = V_{sm}\sin(wt - 120^0) \quad (2.7)$$
$$V_{sc} = V_{sm}\sin(wt + 120^0)$$

Where,

V_{sa}, V_{sb}, V_{sc} are instantaneous voltage phase A, B and C

V_{sm} and w are voltage amplitude and angular frequency

The shunt active power filter operating principle is to inject into the power supply network the same harmonics current as that generated by the nonlinear load but in the opposite direction. The SAPFs are connected in parallel with the harmonic producing loads.

The performance of active power filter depends mainly on the technique used to identify and extract the reference current (harmonic current) and the inverter control strategy (Chelli *et al.*, 2015; Mernis, 2015). The block diagram of shunt active filter in a 3-phase power system is shown in Figure 2.14.

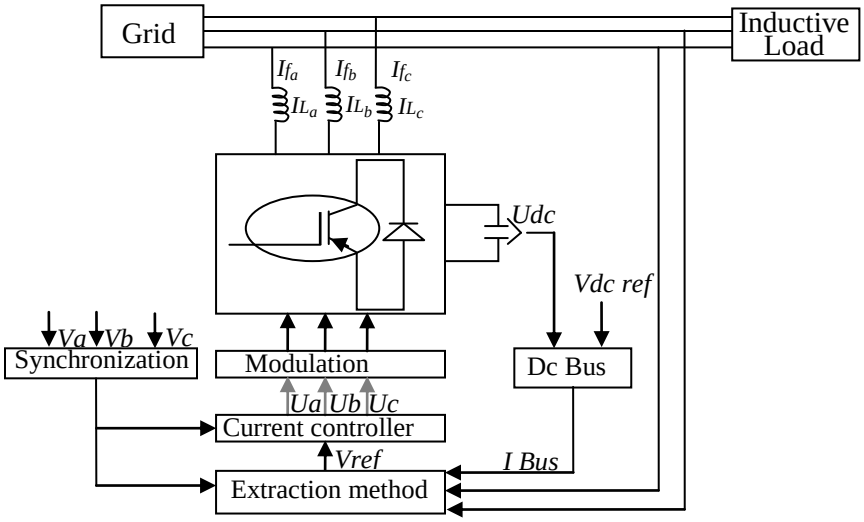


Figure 2.14: Shunt Active Filter Block Diagram (Zahira & Peer, 2011)

Therefore, from the Figure 2.14, source current (I_S) can be written as (Chelli *et al.*, 2015).

$$\mathbf{I_S = I_L - I_f} \tag{2.8}$$

Where,

I_S is source current (rms)

I_f is compensation current or inverter current (rms)

I_L is load current (rms)

2.2.4 Shunt Active Power Filter Parameters Design Approach

Several approaches for designing of the SAPF system parameters have been discussed in literatures. This section discussed the basic design configuration for selecting the appropriate design components for 3-ph and 3-wire distribution system. The components needed in designing the SAPF are DC bus voltage, V_{dc} coupling inductor, L_f and DC capacitor, C_{dc}

2.2.4.1 Dc Voltage,V_{dc}

A working diagram of phase A of the grid at the PCC and compensating power exchange mechanism of the APF is shown in Figure 2.15 (Shafiuzzaman *et al.*, 2014). The $S_{vsi\text{-}h}$ value is calculated from and of the APF_{sh}, (which depends on the V_{sh}, I_f, L_{sh} and f_{sw}) to compensate for specific harmonics, the maximum limit of these values should be considered to determine the maximum acceptable as P_{Loss} well as $S_{vsi\text{-}h.}$ Again, from the study of switching dynamics it is found that the switching frequency is very much dependent on the V_{pcc}, V_{sh} and I_{sh}, L_{sh} and h.

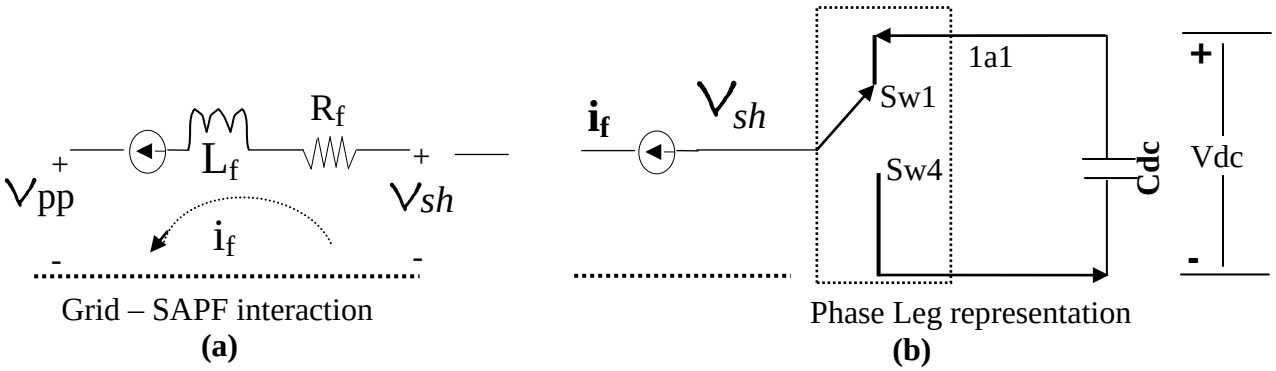


Figure 2.15: Compensating Power Exchange between the Grid and Shunt APF (Shafiuzzaman, 2013)

The maximum harmonic compensation capacity of the APF_{sh} can be written as (Shafiuzzaman *et al.,* 2014).

$$H_{sh\text{-}max} = \frac{3V_{pcc\text{-}max}V_{sh\text{-}max}}{Z_{sh}} \tag{2.9}$$

Also, the main VSI rating for harmonic power compensation of the APF_{sh} can be written as (Shafiuzzaman *et al.*, 2014).

$$S_{vsi\text{-}h} = \sqrt{H_{sh}^2 + p_{loss}^2} \tag{2.10}$$

P_{loss} is the total active power loss of the APF_{sh} during its compensation task which includes conduction loss of interfacing inductor, transformer (if any), VSI and switching loss of VSI. The overall impedance of the APF system is considered as ($j\omega L_f + R_f$), then P_{loss} will be expressed as (Shafiuzzaman *et al.*, 2014).

$$P_{loss} = 3I_f^2 R_f \tag{2.11}$$

Depending on the topology, different methods or approaches have been presented on the relation between V_{pcc}, V_{sh} and V_{dc}. For a 3-ph, 3-wire system, considering the amplitude modulation factor, m_a=1, the minimum value of V_{dc} should be at least equal to $2V_{pcc\text{-}max}$ or $2\sqrt{2}V_{sh}$ or greater than $\sqrt{3}V_{sh\text{-}max}$. Based on this information, the minimum value of V_{dc} can be derived as (Shafiuzzaman, 2013; Marwa *et al.,* 2017)

$$V_{dc} \geq \sqrt{3}V_{pcc\text{-}max} \tag{2.12}$$

2.2.4.2 Coupling Inductor L_f

The selection of smoothing inductance (L_f) directly affects the performance of the active power filter. In order to limit the maximum slope of the current within compensation capability of the active filter, a smoothing has been inserted to prevent inverter saturation (Laith, 2016). The main benefit is to smoothing the wave shape of the current by elimination of the ripples produced in

the current (Shrutisnata, 2016). The inductor should not be large so that it can adjust to track sudden load current variations. It should not be too small to prevent high ripple content (Laith, 2016). The interface inductor design is based on its ability to compensate both reactive power and harmonic current. The inductor required in the active power line conditioner for current control is determined from the constraint on the maximum ripple current, $I_{f\text{-}max}$ (Marwa *et al.*, 2017). In power transistor, the maximum ripple current occurs at the zero-crossings of the fundamental frequency component of the output voltage (Karuppanan, 2012). The minimum value of interfacing inductor is computed as (Shafiuzzaman, 2013; Marwa *et al.*, 2017).

$$Lf \geq \frac{V_{dc}}{12 f_{sw} k I_{f\text{-}max}} \tag{2.13}$$

Where,

$I_{f\text{-}max}$ - Maximum ripple current

K – Limiting maximum current (i.e. 0.05 - 0.15)

f_{sw} – Switching frequency

2.2.4.3 DC Side Capacitor C_{dc}

The design of the DC side capacitor is based on the principle of instantaneous power flow. A resistor is connected in series with the capacitor to protect the VSI from initial high current which could damage the component since the impedance of (X_c) is theoretically zero at the moment filtering energization (Laith, 2016). DC capacitor (C_{dc}) helps to maintain a DC voltage with small ripple in steady state and serves as an energy storage element to supply real power difference between the load and source during the transient period (Shafiuzzaman, 2013).

The value of the capacitor must be higher than the minimum calculated value for capacitor voltage to be maintained constant (Mernis, 2015).

The selection of C_{dc} can be governed by reducing the voltage ripple (Yogesh, 2014). The energy handling capacity determines the size of the capacitor. The basic equation can be written as (Shafiuzzaman, 2013).

$$C_{dc} = \frac{2S.n.T}{V_{dc\text{-}max}^2 - V_{dc\text{-}min}^2} = \frac{2S.n.T}{\{(1+z)V_{dc}\}^2 - \{(1-z)V_{dc}\}^2} = \frac{S.n.T}{2zV_{dc}^2} \quad (2.14)$$

where S is the power required to be compensated during the steady state condition; supplied to the load during the transient condition and absorbed due to the load change during the transient condition. T is the required time period for one complete cycle, *n* is the number of cycles for energy transfer and z is the percentage of V_{dc} to replace the V_{dcmax} and $V_{dcmin,}$ the maximum and minimum allowable V_{dc} respectively to perform the specific task.

2.2.5 Harmonics Current Extraction Strategies

Harmonics current extraction strategies consist of dc voltage control methods and the extraction method. There are two major approaches that have been proposed in the literature for harmonic detection, namely, frequency domain and time domain methods (Rathika & Devaraj, 2011). The time domain methods require less computation and are widely followed for computing the reference current. The two mostly used time domain methods are synchronous reference (d-q-0) theory and instantaneous real-reactive power (p-q) theory (Rathika & Devaraj, 2011).

2.2.5.1 Synchronous Reference Frame (d-q)

The synchronous system theory or d-q theory is predicated on time-domain reference signal estimation techniques. It performs the operation in steady-state or transient state in addition as for generic voltage and current waveforms (Balasubramaniam *et al.,* 2014). Another necessary feature of this theory is the simplicity of the calculations that involves algebraic calculation (Hemachandra *et al.,* 2015).

The essential structure of synchronous reference frame (d-q-0) theory consists of direct (d-q) and inverse (d-q) $^{-1}$ park transformation (Balasubramaniam *et al.,* 2014; Hemachandra *et al.,* 2015). The transformation equation is given as follows: (Sunitha & Kartheck, 2014).

$$\begin{bmatrix} i_d \\ i_q \\ i_0 \end{bmatrix} = \sqrt{\frac{2}{3}} \begin{bmatrix} \cos\theta & \cos(\theta - 120) & \cos(\theta + 120) \\ -\sin\theta & -\sin(\theta - 120) & -\sin(\theta + 120) \\ 1/\sqrt{2} & 1/\sqrt{2} & 1/\sqrt{2} \end{bmatrix} \begin{bmatrix} i_a \\ i_b \\ i_c \end{bmatrix} \quad (2.15)$$

2.2.5.2 Instantaneous Real and Reactive Power (P-Q) Theory

The theory was introduced by Akagi et al. (1983) in Japan (Brahim & Chellali, 2011). This theory based on instantaneous values in three-phase power systems with or without neutral wire, and is valid for steady-state or transitory operations. Instantaneous Power Theory (p-q) theory which consists of an algebraic transformation (Clarke transformation) of the three-phase voltages in the a-b-c coordinates to the α-β coordinates, followed by the calculation of the p-q theory instantaneous power components (Nalini *et al.,* 2011; Umar, 2017).

Instantaneous Power Theory or Active- Reactive (p-q) theory has good transient response time and steady state accuracy, it was found to be not suitable for estimating reference current under non-ideal source voltage conditions (Rathika & Devaraj, 2011; Celli *et al.,* 2015).

2.2.6 Control Strategies in SAPF

The control strategies in SAPF consist of direct current of bus voltage control method and current control strategies.

2.2.6.1 Direct Current Bus Voltage Control Method

The control of the DC voltage of the APF is of great importance because of its main effect on the stability of the compensation system and the harmonic compensation efficiency. The DC voltage must be kept within certain limits to ensure the control of energy transfer between the grid and the APF (Mohamed, 2012).

However, for making the APF normally achieving the required effect, the DC bus voltage has to be high enough and stable (Naresh *et al.,* 2012). Another important task in the development of active filter is the maintenance of constant DC voltage across the capacitor connected to the inverter. This is necessary to compensate the energy loss due to conduction and switching power losses associated with the diodes and IGBTs of the inverter in APF (Rathika *et al.,* 2011). DC bus voltage equation is expressed as (Soomro *et al.* 2015).

$$e = V_{dc\text{-}ref} - V_{dc} \tag{2.16}$$

Where,

e is the voltage error

$V_{dc\text{-}ref}$ is the reference dc bus voltage

V_{dc} is the actual dc bus voltage

2.2.6.2 Current Control Strategies for PWM

Most of the current control techniques used in active power filter is based on PWM-current control strategy. Various PWM-current control strategies such as hysteresis, triangular wave control, dead beat control, PI control, predictive current control, Sliding Mode Control (SMC) have been applied for active power filter applications. Among the various current control techniques, hysteresis control is the most commonly used method because of its simplicity in implementation. But, with fixed hysteresis band, the slope of the reference current is unpredictable, which leads to increase in switching frequency (Rathika & Devaraj, 2011).

Active Power filter must supply the anti-harmonics as per the load requirement (Karuppanan, 2012). The current control techniques should posses the following properties for efficient performance of the active power filter which are: (i) better utilization of the voltage source inverter, for producing high current in a given non-linear load (ii) low static and dynamic current-control errors (difference between the reference current and actual currents is less) (iii)

wide linear modulation range (iv) low amplitudes of lower order harmonics in output voltage to minimize the harmonics in output current; lower switching losses in the power transistor (voltage source inverter) switches and easy implementation and less computation time (Karuppanan, 2012).

2.2.6.3 Sinusoidal Pulse Width Modulation (SPWM)

Pulse width modulation (PWM) strategy plays an important role in the minimization of harmonics and switching losses in converters, especially in three-phase applications. The first modulation techniques were developed in the mid-1960s by Kirnnich, Heinrick, and Bowes (Phuong, 2012). Pulse width modulation is a powerful technique for controlling analogue circuits in digital form with a microprocessor's digital outputs. The key advantage of the PWM techniques is that the ON-OFF behaviors changes the average power of the signal with the output signal alternates between ON and OFF with specified period and therefore, limit the switching power loss (Suleiman *et al.,* 2017). The modulation method in Figure 2.16 below uses a triangular carrier wave, which is one of many methods applied for controlling power inverter (Yogesh, 2014).

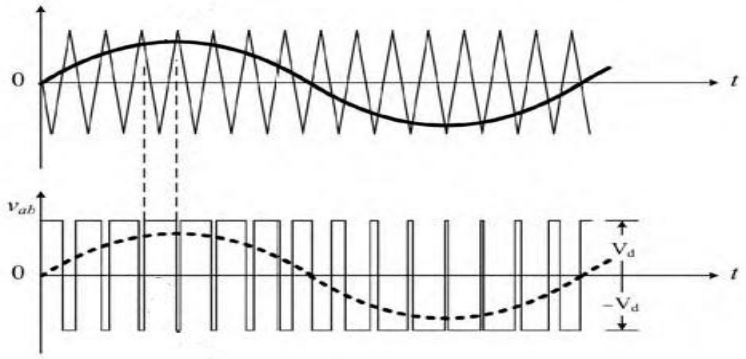


Figure 2.16: Triangular Carrier Pulse Width Modulation Waveform (Bimal, 2006)

2.2.6.4 Space Vector Pulse Width Modulation (SVPWM) Technique

Space vector pulse width modulation (SVPWM) was first introduced in the mid-1980s and was greatly advanced by Van Der Broeck in 1988 (Phuong, 2012).

The main aim of any modulation technique is to obtain a variable output with a maximum fundamental component and minimum harmonics and to lower the switching losses, maximize bus utilization, reduce harmonic content, and still achieve precise control. The SVPWM technique utilizes the DC bus voltage more efficiently and generates less harmonic distortion when compared with the other technique (Kumar *et al.*, 2015, Phuong, 2012).

Space vector pulse width modulation (SVPWM) is a more sophisticated, advanced, computation intensive technique for generating sine wave that provides a higher voltage with lower total harmonic distortion (Irfan *et al.*, 2016).

2.2.6.5 Concept of Space Vector Pulse Width Modulation (SVPWM)

SVPWM technique was originally developed as a vector approach to pulse width modulation for three-phase inverters. Space vector pulse width modulation (SVPWM) is accomplished by rotating a reference vector around the state diagram, which is composed of six basic non-zero vectors forming a hexagon. Figure 2.17 shows the maximum control voltage using sine wave pulse modulation of $1/2\,V_{dc}$ and space vector pulse width modulation of $1/\sqrt{3}V_{dc}$. The area inside the inscribed circle is called the linear modulation region or under-modulation region. The area between the inside circle and outside circle of the hexagon is called the nonlinear modulation region or over-modulation region (Phuong, 2012). The maximum modulation index for the SPWM method is 0.785 with the sinusoidal waveform between the phase and the neutral current of the system. However, the modulation index can be increased to 0.907 for the SVPWM. The

basic principle of the SVM technique is that it treats the inverter as a whole unit, which is different when compared to PWM technique.

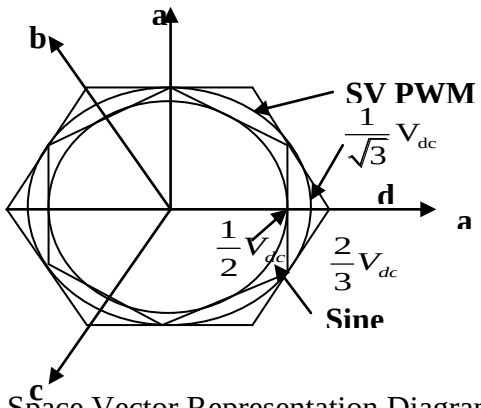


Figure 2.17: Space Vector Representation Diagram (Kumar *et al.*, 2015)

Given a set of three-phase voltages, a space vector can be defined as (Phuong, 2012).

$$\vec{V}(t) = \frac{2}{3}[V_a(t)e^{j0} + V_b(t)e^{j\frac{2\pi}{3}} + V_c(t)e^{j\frac{4\pi}{3}}]V_{dc} \qquad (2.17)$$

Where, $V_a(t)$, $V_b(t)$, and $V_c(t)$ are three sinusoidal voltages of the same amplitude and frequency but with $\pm 120^0$ phase shifts. In the space-vector modulation, a three-phase two-level inverter can be driven to eight switching states where the inverter has six active states (1-6) and two zero states 0 and 7 (Naresh & Prabhat, 2012; Phuong, 2012).

A typical two-level inverter has six power switches that generate three phase voltage outputs. A detailed drawing of a three-phase bridge inverter is shown in the Figure 2.16. When an upper transistor is switched on, the corresponding lower transistor is switched off.

Therefore, the ON and OFF states of the upper transistors S_1, S_3 and S_5 can be used to determine the current output voltage (Naresh & Prabhat, 2012). The output pole voltages Vao, Vbo, and Vco of the inverter switch between -Vdc=2 and +Vdc=2 voltage levels where Vdc is the total DC voltage. Depending on the switching states, either the positive or negative half DC bus

voltage is applied to each phase (Phuong, 2012**)**. The switches are controlled in pairs as [(S1; S4), (S3; S6), and (S5; S2)].

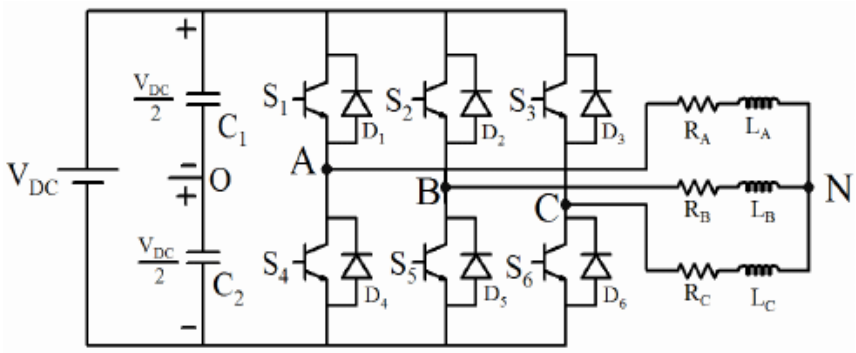


Figure 2.18: Three Phase Inverter Block Diagram (Phuong, 2012**)**

There are eight possible inverter states that can generate eight space vectors. Figure 2.19 shows the eight switching configuration of a three-phase inverter (Phuong, 2012; Kumar *et al.,* 2015; Naresh & Prabhat, 2012).

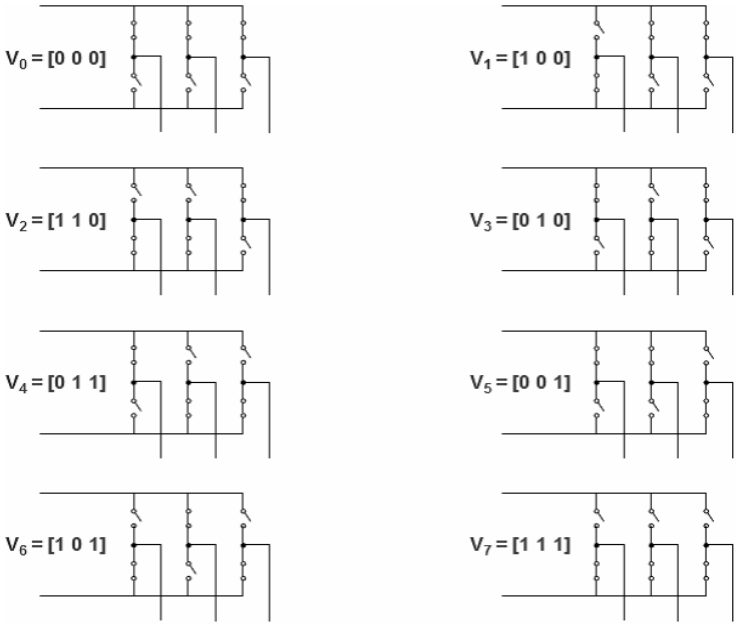


Figure 2.19: Switching Configuration of a Three-Phase Inverter (Priyanka & Shruti, 2017)

The reference voltage vector $\vec{V}_{ref}$ rotates in space at an angular velocity $\omega = 2\pi f$, where f is the fundamental frequency of the inverter output voltage. Figure 2.20 shows the reference vector $\vec{V}_{ref}$ in the first sector (Phuong, 2012).

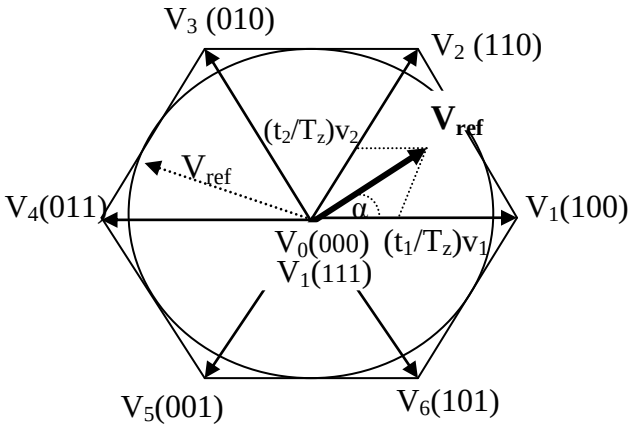


Figure 2.20: Space Vectors of Three-Phase Bridge Diagram (Thamizhazhagan & Shuha, 2015**)**

The entire space is divided into six equal-size sectors of 60^o. Each sector is bounded by two active vectors. $\vec{V}_0$ and $\vec{V}_7$ are two voltage vectors with zero amplitude located at the origin of the hexagon.

When the reference voltage vector passes through each sector, different sets of switches in Table 2.1 will be turned on or off (Phuong, 2012).

Table 2.1: Space Vectors, Switching States, and On State Switches (Phuong, 2012)

Space Vector	Switching State	On-state Switch	Vector Definition
$\overrightarrow{V_0}$	[000]	S4, S6, S2	$\overrightarrow{V}_0 = 0$
$\overrightarrow{V_1}$	[100]	S1, S6, S2	$\overrightarrow{V}_1 = \frac{2}{3} V_{dc} e^{j0}$
$\overrightarrow{V_2}$	[110]	S1, S3, S2	$\overrightarrow{V}_2 = \frac{2}{3} V_{dc} e^{j\frac{\pi}{3}}$
$\overrightarrow{V_3}$	[010]	S4, S3, S2	$\overrightarrow{V}_3 = \frac{2}{3} V_{dc} e^{j\frac{2\pi}{3}}$
$\overrightarrow{V_4}$	[011]	S4, S3, S5	$\overrightarrow{V}_4 = \frac{2}{3} V_{dc} e^{j\frac{3\pi}{3}}$
$\overrightarrow{V_5}$	[001]	S4, S6, S5	$\overrightarrow{V}_5 = \frac{2}{3} V_{dc} e^{j\frac{4\pi}{3}}$
$\overrightarrow{V_6}$	[101]	S1, S6, S5	$\overrightarrow{V}_6 = \frac{2}{3} V_{dc} e^{j\frac{5\pi}{3}}$
$\overrightarrow{V_7}$	[111]	S1, S3, S5	$\overrightarrow{V}_7 = \frac{2}{3} V_{dc} e^{j\frac{6\pi}{3}}$

The relationship between the switching variable vector $[a, b, c]$ and line-to-line voltage vector $[V_{ab}, V_{bc}, V_{ca}]$ is given as (Irfan *et al.*, 2016).

$$\begin{bmatrix} V_{ab} \\ V_{bc} \\ V_{ca} \end{bmatrix} = V_{dc} \begin{bmatrix} 1 & -1 & 0 \\ 0 & 1 & -1 \\ -1 & 0 & 1 \end{bmatrix} \begin{bmatrix} a \\ b \\ c \end{bmatrix} \tag{2.18}$$

Also, the relationship between the switching variable vector $[a, b, c]$ and the phase voltage vector $[V_{an}, V_{bn}, V_{cn}]$ can be expressed as (Irfan *et al.*, 2016).

$$\begin{bmatrix} V_{an} \\ V_{bn} \\ V_{cn} \end{bmatrix} = \frac{V_{dc}}{3} \begin{bmatrix} 2 & -1 & -1 \\ -1 & 2 & -1 \\ -1 & -1 & 2 \end{bmatrix} \begin{bmatrix} a \\ b \\ c \end{bmatrix} \tag{2.19}$$

According to equations 2.18 and 2.19 the eight switching vectors, output line to neutral voltage and output line to line voltages with reference to dc-link V_{dc}, are given in Table 2.2 (Phuong, 2012)

Table 2.2**:** Switching Vectors, Phase Voltages and Output Line to Line Voltages (Phuong, 2012)

Space Vector	Switching Vector			Line to Neutral Voltage			Line to Line Voltage		
	a	b	C	V_{an}	V_{bn}	V_{cn}	V_{ab}	V_{bc}	V_{ca}
$\vec{V_0}$	0	0	0	0	0	0	0	0	0
$\vec{V_1}$	1	0	0	2/3	-1/3	-1/3	1	0	-1
$\vec{V_2}$	1	1	0	1/3	1/3	-2/3	0	1	-1
$\vec{V_3}$	0	1	0	-1/3	2/3	-1/3	-1	1	0
$\vec{V_4}$	0	1	1	-2/3	1/3	1/3	-1	0	1
$\vec{V_5}$	0	0	1	-1/3	-1/3	2/3	0	-1	1
$\vec{V_6}$	1	0	1	1/3	-2/3	1/3	1	-1	0
$\vec{V_7}$	1	1	1	0	0	0	0	0	0

The SVPWM scheme is more complicated than that of the conventional SPWM. It requires the determination of a sector, calculation of vector segments, and it involves region identification based on the modulation index and calculation of switching time durations (Phuong, 2012).

2.3 Review of Similar Works

Some literatures relevant to shunt active power filter (SAPF) are described in this section.

Kale & Ozdemir (2013) developed a new hysteresis band (HB) current control technique to reduce the power losses in a shunt active power filter. In this research work, a zero- crossing regions during a fundamental frequency cycle was avoided. The result for the proposed method is 4.77% THD. The extraction method used was instantaneous reactive power theory. The hysteresis current controller method used has low switching frequency which resulted to slow dynamic response.

Soomro *et al.*, (2013) designed an application of three-phase shunt active power filter (SAPF) using active and reactive power (p-q) theory as control strategy to mitigate harmonics and power factor correction was presented. Hysteresis current controller (HCC) was used as a current controller. DC-link voltage is maintained using proportional integral (PI) controller. The result of the method is 1.77% (THD) and 0.9993 power factor. The hysteresis current controller method used was known for uneven switching pulse generation which causes switching power losses of the inverter.

Sunitha & Kartheck (2013) developed a method of maintaining reference current for shunt active power filter (SAPF) using synchronous reference frame (SRF) as a control method. Sinusoidal pulse width modulation (SPWM) was used switching signal generation. DC-link voltage was maintained using proportional integral (PI) controller. Sinusoidal pulse width modulation (SPWM) has a narrow range of modulation index which limits it harmonics reduction capability.

Rama & Sobharani (2014) discussed a shunt active power filter (SAPF) for mitigating the power quality problem using instantaneous active and reactive current component (id-iq) control strategy. Pulse width modulation (PWM) was used for the control of compensation current. DC-

link voltage was maintained using proportional integral (PI) controller. The result of the method is 3.77% (THD). Sinusoidal pulse width modulation (SPWM) is also known for high harmonic component frequency generation which leads to harmonics distortion of the inverter.

Varaprasad & Siva (2014) developed an improved space vector pulse width modulation (SVPWM) techniques based on shunt active power filter (SAPF) using synchronous reference frame (SRF) theory as a control method. DC-link voltage was maintained using proportional integral (PI) controller. The result of the method is 4.47% (THD). Space vector pulse width modulation (SVPWM) is a more sophisticated though it has computational complexity. SVPWM has a wide range of modulation index which allows it to have a wider range of harmonics reduction capability.

Chenai & Benchouia (2014) developed a shunt active power filter (SAPF) performances based on three level (NPC) inverter using conventional pulse width modulation (PWM) logic controller and artificial neural network (ANN) as a switching signal generation techniques. The control strategy used was proportional integral (PI) controller with synchronous current detection (SD) method. The results of ANN (3.96%) showed little improvement over the PWM (4.32%) method. ANN algorithm requires starting values for the angles which does not always converge to the required solution.

Balasubramaniam *et al.*, (2014) proposed a method of maintaining reference current of the shunt active power filter (SAPF) using synchronous reference frame (SRF) as a control method was discussed in the paper. Hysteresis current controller (HCC) is used as a current controller. DC-link voltage was maintained using proportional integral (PI) controller. The result of the method was 2.72% (THD). The hysteresis current controller method used was known for uneven switching pulse generation which leads to power losses of the inverter and acoustic noise.

Venkata *et al.*, (2014) developed the design of shunt active power filter (SAPF) for development of power quality using instantaneous active and reactive power (p-q) theory as a control method. Hysteresis current controller (HCC) was used to generate switching pulse. DC-link voltage was maintained using proportional integral (PI) controller based artificial neural network and proportional integral (PI) controller based particle swarm optimization techniques. The result for PI-ANN is 2.34% (THD) and PI-PSO is 1.66% (THD). The hysteresis current controller method used was known for high switching frequency which causes distortion at the inverter output.

Akash & Makund (2015) developed shunt active power filter (SAPF) was discussed for steady load condition using hysteresis current controller (HCC) and sinusoidal pulse width modulation (SPWM) as current control techniques. Synchronous reference frame (SRF) was used as a control method. DC-link voltage was maintained using proportional integral (PI) controller. The result of the method is 1.17% (THD). The hysteresis current controller method used was known for uneven switching pulse generation. Sinusoidal pulse width modulation (SPWM) was also known for high harmonic component frequency generation and therefore has more harmonics distortion at the output waveform.

Kumar *et al.*, (2015) discussed a reference current generation using self tuning filter (STF) method with instantaneous active and reactive power (p-q) theory. The reference currents generated was further used to generate gate pulses for inverter. This method reduced the harmonic to 4.98%. The switching pulse generation method used was not stated.

Soomro *et al.*, (2015) developed a design and application of three-phase shunt active power filter (SAPF) using proportional integral (PI) with instantaneous active and reactive power (p-q) theory as control strategy to mitigate harmonics and power factor correction. Hysteresis current controller (HCC) was used as a current controller. The result of the method is 1.77% (THD) and

0.9993 power factor. The hysteresis current controller method used was known for uneven switching pulse generation which leads switching losses at the inverter output.

Chelli *et al.*, (2015) developed an improved performance of shunt active power filter (SAPF) to compensate for harmonic distortion in three phase four-wire system. A novel instantaneous active and reactive power (p-q) theory is used as a control strategy based on phased locked loop (PLL) for unbalance main voltages to control shunt active power filter (SAPF). Hysteresis current control was used to generate switching pulse signal for the gate. The results of the method were 1.69%, 1.89% and 1.85% (THD) for phase A, B and C. The hysteresis current controller method also has an uneven switching pulse generation due to high switching frequency generation.

Kumar (2015) developed the application of space vector pulse width modulation (SVPWM) based hysteresis current control techniques as switching signal generation method for shunt active power filter (SAPF) to eliminate current harmonics and improved the power factor. Instantaneous active and reactive power (p-q) theory was used as control strategy. DC-link voltage was maintained using proportional integral (PI) controller. Space vector pulse width modulation (SVPWM) was used to make the fixed switching pattern associated with hysteresis band to be variable, therefore sacrificed the high dynamic response for low response.

SVPWM is known for its computational complexity, though is more sophisticated because of its harmonics current compensation capability. This is due to the fact that the switching technique defines the state of all the inverter as one block.

Irfan *et al.*, (2016) developed an efficient Space vector pulse width modulation (SVPWM) for shunt active power filter (SAPF) as current controller. The performance of SVPWM and PWM was compared using instantaneous active and reactive power (p-q) theory as a control strategy.

Space vector pulse width modulation (SVPWM) is a more sophisticated though it has trigonometric computational complexity. SVPWM has a wide range of modulation index which allows it to have a wider range of harmonics reduction capability.

Prakash *et al.*, (2016) developed a proportional integral artificial neural network for the extraction method (PI-ANN). Hysteresis current controller (HCC) was used as switching signal generation for the inverter. The performance of the proposed controller was compared with Proportional integral instantaneous active and reactive current component (PI-id-iq) control method under balanced and unbalanced sinusoidal voltage condition. The result of the proposed method is 0.97% (THD). The hysteresis current controller method also has an uneven switching pulse generation due to high switching frequency generation.

Abhijit & Kompelli (2016) developed a shunt active power filter (SAPF) for harmonic current elimination using synchronous reference frame (SRF) theory as control strategy. DC-link voltage is maintained using fuzzy logic controller. Hysteresis current controller (HCC) was used to generate switching pulse for the inverter. The result of the method used is 1.75% (THD). The hysteresis current controller method also has an uneven switching pulse generation due to high switching frequency generation.

Akash *et al.*, (2016) developed fuzzy logic controller for DC-link voltage regulation for shunt active power filter (SAPF). Instantaneous active and reactive power (p-q) theory was used as control strategy. Hysteresis current controller was used to generate the gate pulse for the inverter. The result of the method used is 1.66% (THD). The hysteresis current controller method also has an uneven switching pulse generation due to high switching frequency generation.

Rama *et al.*, (2016) developed an approach to determine reference current of three phase shunt active power filter (SAPF) using synchronous reference frame (SRF) control strategy. Hysteresis

band current control was used for switching pulse signal generation. The result of the method used is 3.32% (THD) for diode bridge rectifier and 4.35% (THD) for thyristor bridge rectifier. The switching frequency of the hysteresis current controller method used is high and therefore leads to switching power losses and acoustic noise.

Niklesh & Sandeep (2017) discussed a shunt active power filter (SAPF) based on instantaneous active and reactive power (p-q) theory and instantaneous active and reactive current component (id-iq) techniques as control strategy. Hysteresis band current control was used for switching pulse signal generation. DC-link voltage was maintained using proportional integral (PI) controller. The hysteresis current controller method also has an uneven switching pulse generation due to high switching frequency generation.

Shashibhushan & Nikhil (2017) developed shunt active power filter (SAPF) was compared for steady load condition for both hysteresis current controller (HCC) and sinusoidal pulse width modulation (SPWM) as current control techniques. Synchronous reference frame (SRF) was used as a control method. DC-link voltage was maintained using proportional integral (PI) controller. SPWM achieved a harmonic reduction of 2.17%. The hysteresis current controller method used was known for uneven switching pulse generation. Sinusoidal pulse width modulation (SPWM) was also known for high harmonic component frequency generation and therefore has more harmonics distortion at the output waveform.

Suleiman *et al.*, (2017) developed a modified synchronous reference frame (MSRF) as a control strategy for three phase shunt active power filter (SAPF). Fuzzy logic controller (FLC) based current control pulse width modulation (PWM) was used to generate switching signal for the inverter. The result was 0.92 %THD. The major drawback of fuzzy logic controller is over dependency on the expert knowledge which may not be available or accurate most time and this

make the development of a fuzzy logic controller become time consuming and tedious or sometimes impossible.

Mohamed *et al.*, (2017) developed control strategy that combines synchronous reference frame and the unit vector template generation method for shunt active power filters for harmonic reduction. The result of the method used is 3.87% (THD) and the result of the technique was validated using IEEE-519 Standard. The switching frequency of the hysteresis current controller method used is high and therefore leads to switching power losses and acoustic noise.

Abdeldjabbar & Tayeb (2017) proposed a fuzzy hysteresis band technique for the current control for shunt active power filter (SAPF) was discussed. The control strategy for reference current generation was proportional integral (PI) controller with instantaneous active and reactive power (p-q) theory. The result of the method used is 1.08% (THD), though the result is still within the IEEE-519 Standard. The work did not consider unbalanced voltage condition. Fuzzy logic was used to make the fixed switching pattern associated with hysteresis band to be variable, therefore sacrificed the high dynamic response for low response.

The literatures reviewed showed that harmonics reduction have been given a significant attention in the field of power engineering. The authors showed that most of the work done on harmonic reduction is based on balanced sinusoidal voltage source which does not occur often in reality. However, Shunt active power filter (SAPF) is presented in this work, using synchronous reference frame as harmonic current extraction method and space vector pulse width modulation (SVPWM) current controller as current controller to eliminate high harmonic component frequency generation and narrow range of modulation index in sinusoidal pulse width modulation (SPWM). Harmonics compensation under both balanced and unbalanced sinusoidal voltage conditions was considered for both RL and RC non linear loads.

CHAPTER THREE

METHODOLOGY

3.1 Introduction

The methods for designing a three-phase three-wire Shunt Active Power Filter (SAPF) based on VSI are presented in this chapter. The controller is categorized into three parts, extraction of reference signal generation, DC bus voltage control and current control. Strategies to generate compensation commands are implemented in time-domain techniques.

3.2 Methodology

The objectives of this work were achieved with the following steps.

1. Design of a shunt active power filters parameters. The parameters are as follows:
    (i) Selection of DC bus voltage
    (ii) Selection of coupling inductor
    (iii) Selection of DC storage capacitor
2. Design of control Strategy method for reference signal generation using synchronous reference frame (SRF) theory.
3. Design of space vector pulse width modulation (SVPWM). The procedures are as follows:
    (i) Determination of V_d, V_q, V_{ref} and angle α
    (ii) Determination of time duration T_0, T_1 and T_2
    (iii) Determination of switching time of each transistor (S_1- S_6)

3.3 Selection of Shunt Active Power Filter Design Parameters

The selection of shunt active power filter is based on the design approach presented and detailed in Section 2.2.4, the initial target of maximum harmonic compensating current, I_{fmax}, has been set at 100A which requires an APF_{sh} of 48.8 kVA rated capacity (H_{sh}) in a $400V_{(p-p)}$ distribution system. The fswmax of IGBT limit is around 20 kHz. The wide range of values of I_{fmax}, h, L_f, R_f and V_{dc} have been chosen to calculate the VSI power rating, S_{vsi-h} and P_{loss} for harmonic compensation using equation 2.10 and 2.11. The connection topology and switching configuration of a 3-ph, 3-wire APF_{sh} together with the generalized chosen parameters range is shown in Figure 3.1.

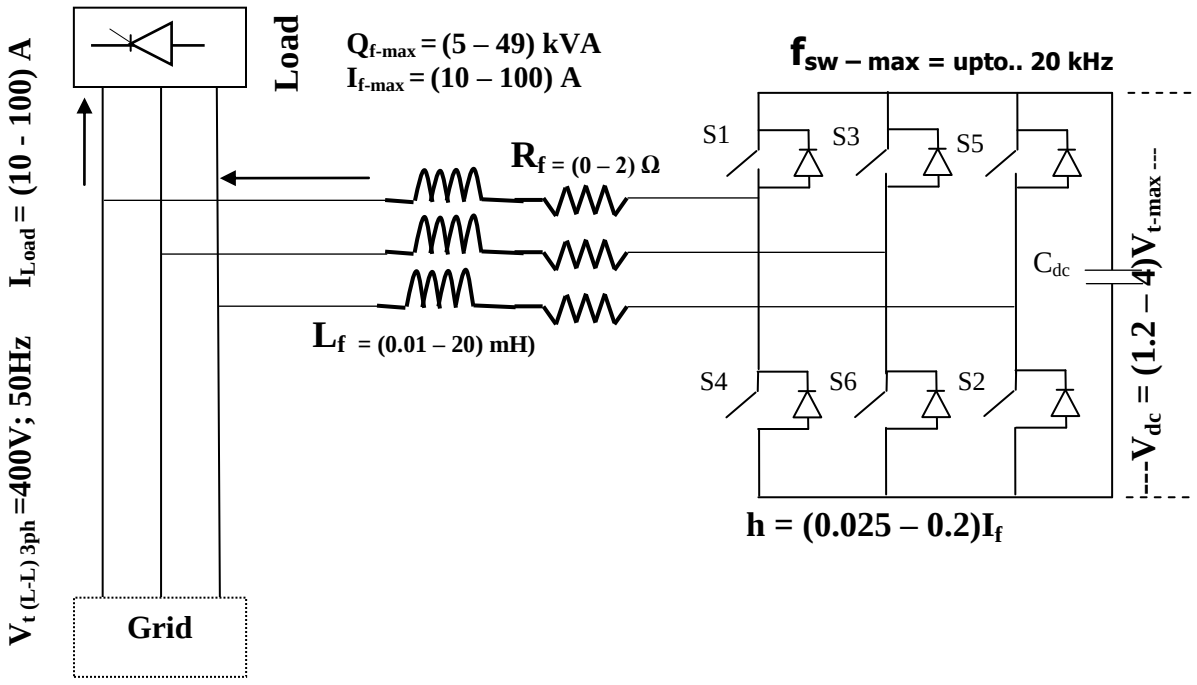


Figure 3.1: A 3-ph, 3-wire SAPF connected to the grid and load at PCC

3.3.1 Selection of DC Reference Voltage

The minimum value of Vdc was calculated using equation 2.12 (Shafiuzzaman, 2013)

$$V_{dc} \geq \sqrt{3}Vpcc - max$$

Vpcc-max = 400V

The required minimum of V_{dc} was calculated to be 693V. Therefore, 700V was chosen.

3.3.2 Selection of Coupling Inductor

The minimum value of L_f was calculated using equation 2.13 (Shafiuzzaman, 2013)

$$Lf \geq \frac{V_{dc}}{12fswkI_{f-max}}$$

The converter maximum ripple current = 10A

Vdc = 693V (for modulation index = 1.7)

Switching frequency = 20 KHz.

The minimum value of L_f was calculated to be 2.88mH. Therefore, 3mH was chosen.

3.3.3 Selection of DC Side Capacitor

The minimum value of C_{dc} was calculated using (2.14) (Shafiuzzaman, 2013)

$$C_{dc} = \frac{2S.n.T}{V_{dc-max}^2 - V_{dc-min}^2} = \frac{2S.n.T}{\{(1+z)V_{dc}\}^2 - \{(1-z)V_{dc}\}^2} = \frac{S.n.T}{2zV_{dc}^2}$$

The allowable compensator power transfer is 20kVA

Number of cycle, n = 0.5 (i.e. half cycle)

Period, T for one complete cycle is 0.02Sec

Change in Vdc of 10% (i.e. z = 0.1)

Vdc = 693V (for modulation index = 1.7)

The minimum capacity of C_{dc} was calculated to be 2082µF. Therefore, 3000µF was chosen.

The design SAPF parameters is therefore summarized in Table 3.1 (Suleiman *et al.*, 2017)

Table 3.1 SAPF Parameters (Suleiman *et al.*, 2017)

PARAMETER	VALUE
SUPPLY	$V_S = 220V$, $F_S = 50H_Z$, $R_S = 0.15\Omega$ $L_S = 0.03mH$
LOAD INDUCTANCE	$R_L = 40\Omega$, $L_L = 2mH$
SAPF	$V_{dc} = 700$, $L_C = 3mH$, $C_{dc} = 3000\mu F$

3.4 Modeling of Shunt Active Power Filter in d-q

The SRF method is implemented by transforming the three-phase source Va, Vb and Vc and load current i_a , i_b , and i_c into the three-phase (d-q-0) synchronous reference frame in DC quantities as expressed as

$$\begin{bmatrix} i_d \\ i_q \\ i_0 \end{bmatrix} = \sqrt{\frac{2}{3}} \begin{bmatrix} \cos\theta & \cos(\theta-120) & \cos(\theta+120) \\ -\sin\theta & -\sin(\theta-120) & -\sin(\theta+120) \\ 1/\sqrt{2} & 1/\sqrt{2} & 1/\sqrt{2} \end{bmatrix} \begin{bmatrix} i_a \\ i_b \\ i_c \end{bmatrix} \quad (3.1)$$

The voltage equation for each phase of the three phase shunt active power filter is expressed as (Mohammed, 2012).

$$L_f \frac{di_a}{dt} = V_{fa} - R_f i_{fa} - V_{sa} \tag{3.2}$$

$$L_f \frac{di_b}{dt} = V_{fb} - R_f i_{fb} - V_{sb} \tag{3.3}$$

$$L_f \frac{di_c}{dt} = V_{fc} - R_f i_{fc} - V_{sc} \tag{3.4}$$

$$C_{dc} \frac{dV_{dc}}{dt} = S_a i_{fa} + S_b i_{fb} + S_a i_{fc} \tag{3.5}$$

Equations 3.2 to 3.5 are transformed to synchronous reference frame using equation 3.1. as expressed as

$$L_f \frac{di_{fd}}{dt} = V_{fd} - V_{sd} - R_f i_{fd} - L_f \omega i_{fq} \tag{3.6}$$

$$L_f \frac{di_{fq}}{dt} = V_{fq} - V_{sq} - R_f i_{fq} + L_f \omega i_{fd} \tag{3.7}$$

$$C_{dc} \frac{dV_{dc}}{dt} = S_d i_{fd} + S_q i_{fq} \tag{3.8}$$

Figure 3.2 shows a low pass filter (LPF) is connected immediately after the SRF to separate fundamental harmonic from harmonic load current.

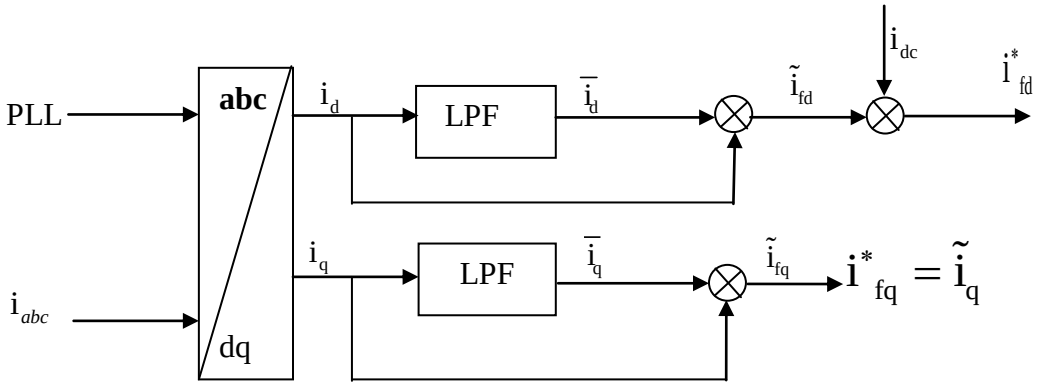


Figure 3.2: Block Diagram of Principle of the Synchronous Reference Method

Harmonics with DC quantities are transformed entirely into non-DC quantities at appropriate corner frequency are shown as (Rama & Sobharani, 2014; Suleiman *et al.,* 2017).

$$\begin{bmatrix} \mathbf{i}_d \\ \mathbf{i}_q \end{bmatrix} = \begin{bmatrix} \overline{\mathbf{i}_d} & \tilde{\mathbf{i}}_d \\ \overline{\mathbf{i}_q} & \tilde{\mathbf{i}}_q \end{bmatrix} \tag{3.9}$$

Where,

$\overline{i}_d$ and $\overline{i}_q$ - fundamental harmonic in d and q axis

$\tilde{i}_d$ and $\tilde{i}_q$ - distorted harmonic in d and q axis

The shunt active power filter extracted reference current therefore expressed as

$$\begin{bmatrix} \mathbf{i}^*_{fd} \\ \mathbf{i}^*_{fq} \end{bmatrix} = \begin{bmatrix} \tilde{\mathbf{i}}_d \\ \tilde{\mathbf{i}}_q \end{bmatrix} \tag{3.10}$$

Where,

i^*_{fd} - Reference current in d axis

i^*_{fq} - Reference current in q axis

3.4.1 Control in Synchronous Frame Reference (d-q)

Proportional Integral (PI) controller is used to directly control the current in the synchronous reference frame (d-q) as shown in Figure 3.3. (Mohammed, 2012).

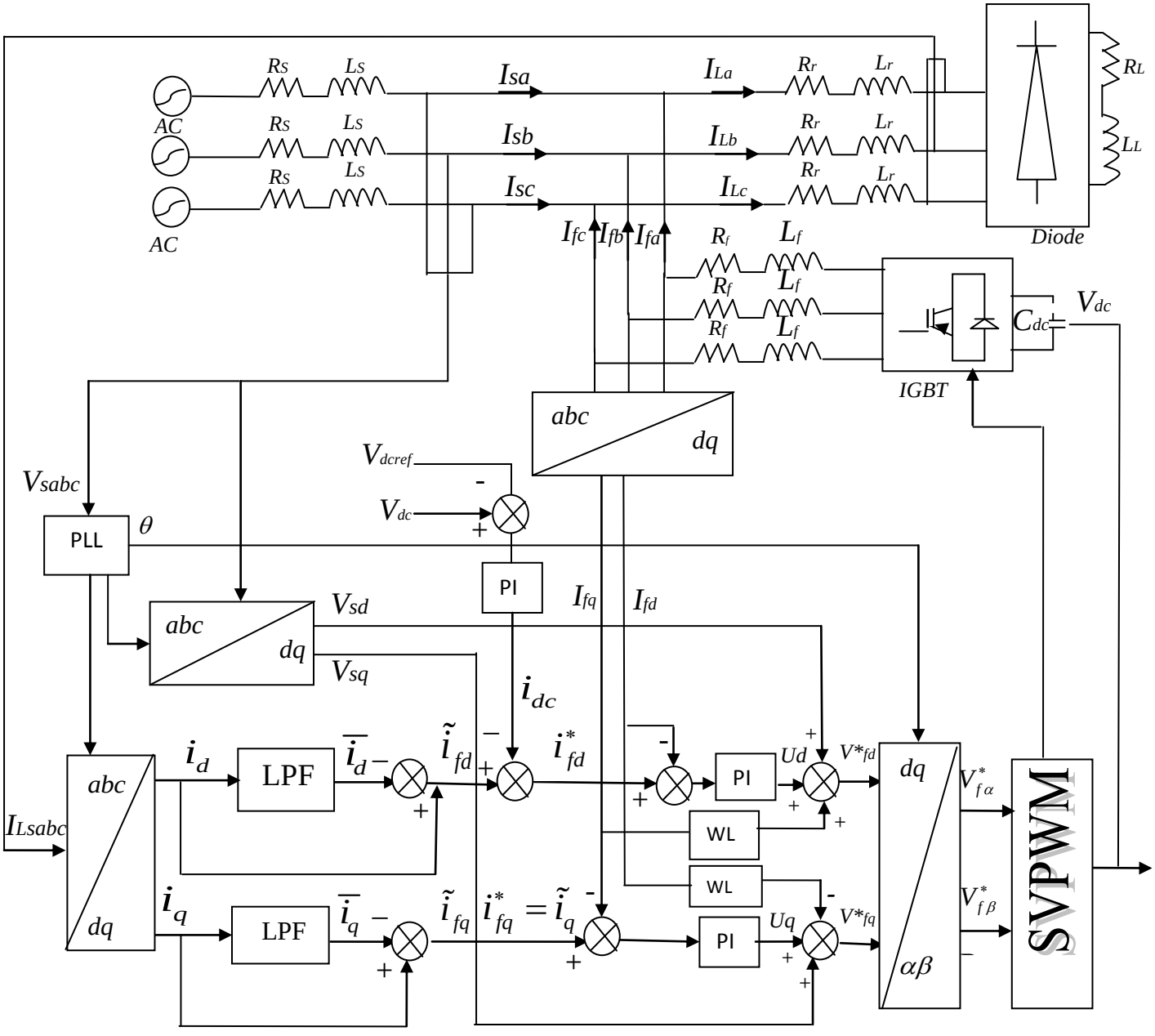


Figure 3.3: Direct Control by PI Controllers in the Synchronous Reference (Mohammed, 2012)

Equation 3.6 to 3.8 is re-arranged as expressed as

$$V_{sd} = V_{fd} - R_f i_{fd} - L_f \frac{di_{fd}}{dt} - L_f \omega i_{fq} \tag{3.11}$$

$$V_{sq} = V_{fq} - R_f i_{fq} - L_f \frac{di_{fq}}{dt} + L_f \omega i_{fd} \tag{3.12}$$

$$C_{dc} \frac{dV_{dc}}{dt} = S_d i_{fd} + S_q i_{fq} \tag{3.13}$$

The currents on the axes d and q are decoupled into two components as

$$U_d = L_f \frac{di_{fd}}{dt} + R_f i_{fd} \tag{3.14}$$

$$U_q = L_f \frac{di_{fq}}{dt} + R_f i_{fq} \tag{3.15}$$

Therefore, equation 3.14 and 3.15 is re-written as expressed as

$$V_{fd}^* = U_d + V_{sd} + L_f \omega i_{fq} \tag{3.16}$$

$$V_{fq}^* = U_q + V_{sq} + L_f \omega i_{fd} \tag{3.17}$$

Equation 3.16 and 3.17 was model in MATLAB/SIMULINK as shown in Figure 3.4

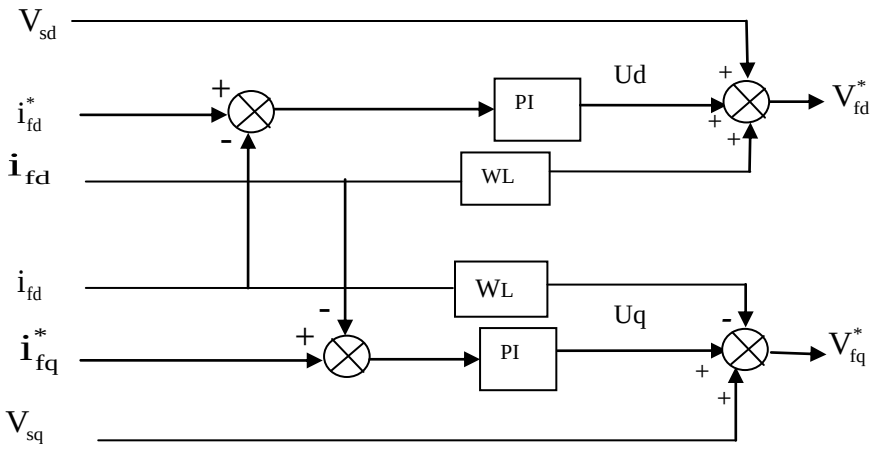


Figure 3.4: Current Controllers in Synchronous Reference Block Diagram

3.4.2 DC Bus Control Using PI

The control of DC bus is done by comparing the actual capacitor voltage with a set reference value. The error signal is then processed through a PI controller, which contributes to zero steady error in tracking the reference current signal. The output of the PI controller is taken as peak value of the supply current (I), which is composed of fundamental active power component of load current and loss component of APF (Rahul, 2014). The control of DC bus derived as expressed as follow (Mohammed, 2012).

Neglect the losses in the inverter and the output filter, the relation between the absorbed power by the filter and the voltage around the capacitor can be given as (Mohammed, 2012).

$$P_{dc} = \frac{d}{dt}\left(\frac{1}{2}C_{dc}V_{dc}^2\right) \tag{3.18}$$

By applying the laplace transformation to the equation 3.18, is expressed as

$$P_{dc} = \frac{1}{2}SC_{dc}V_{dc}^2 \tag{3.19}$$

Therefore, the capacitor voltage is given as

$$V_{dc}^2 = \frac{2P_{dc}}{C_{dc}S} \tag{3.20}$$

The control loop of DC voltage is represented in Figure 3.5

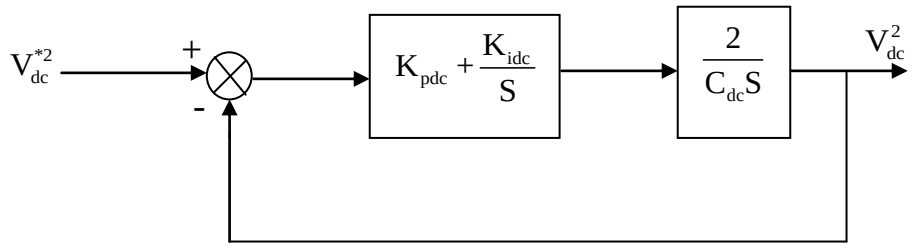


Figure 3.5: DC Voltage Control Loop Block Diagram.

The control transfer function is therefore written as

$$H(s) = \frac{(1 + \frac{k_{pdc} S}{K_{idc}})}{S^2 + 2\frac{k_{pdc}}{c_{dc}} S + 2\frac{k_{idc}}{c_{dc}}} \tag{3.21}$$

The PI controller parameters are therefore derived as

$$k_{idc} = \frac{1}{2} C_{dc} \omega_c^2 \tag{3.22}$$

$$k_{pdc} = \xi \sqrt{2 C_{dc} k_{idc}} \tag{3.23}$$

Where,

$$\omega_c = 2\pi f_c \tag{3.24}$$

3.5 Design of Space Vector Pulse Width Modulation (SVPWM)

Space vector pulse width modulation can be implemented by the following steps

(i) Determination of V_d, V_q, V_{ref} and angle α

(ii) Determination of Time Duration T_0, T_1 and T_2

(iii) Determination of switching time of each transistor $(S_1 - S_6)$

3.5.1 Determination of V_d, V_q, V_{ref} and Angle α

Determination of V_d, V_q, V_{ref} and angle α is derived as follows: (Mohammed, 2012; Renu *et al.*, 2016; Jin-Woo, 2015).

Consider the sector 1 of the space vector hexagonal diagram in Figure 3.6.

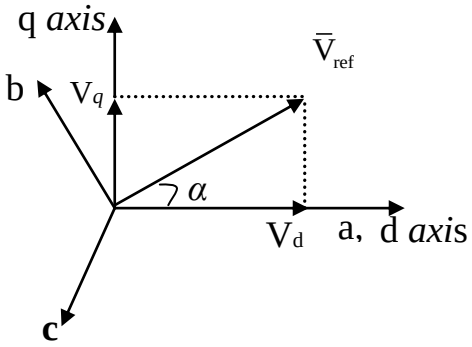


Figure 3.6: Voltage Space Vector and its Components in (D- Q)

Direct voltage equation and quadrature voltage equation can be written as

$$V_d = V_{an} - V_{bn}\cos 60 - V_{cn}\cos 60 = V_{an} - \frac{1}{2}V_{bn} - \frac{1}{2}V_{cn} \tag{3.25}$$

$$V_q = 0 + V_{bn}\cos 30 - V_{cn}\cos 30 = 0 + \frac{\sqrt{3}}{2}V_{bn} - \frac{\sqrt{3}}{2}V_{cn} \tag{3.26}$$

Equation 3.25 and 3.26 can be re-written in matrix form as

$$\begin{bmatrix} V_d \\ V_q \end{bmatrix} = \frac{2}{3}\begin{bmatrix} 1 & -\frac{1}{2} & -\frac{1}{2} \\ 0 & \frac{\sqrt{3}}{2} & -\frac{\sqrt{3}}{2} \end{bmatrix} \tag{3.27}$$

Also equation of the alpha voltage and beta voltage is given as

$$\begin{bmatrix} V_\alpha \\ V_\beta \end{bmatrix} = \begin{bmatrix} \cos\theta & -\sin\theta \\ \sin\theta & \cos\theta \end{bmatrix} \tag{3.28}$$

Therefore, reference voltage equation and alpha angle are written as

$$|V_{ref}| = \sqrt{V_\alpha^2 + V_\beta^2} \tag{3.29}$$

$$\alpha = \tan^{-1}\left(\frac{V_\alpha}{V_\beta}\right) = \omega t \tag{3.30}$$

Where,

α - Angle between reference voltage and alpha voltage

Equations 3.25, 3.26, 3.29 and 3.30 was written as algorithm in MATLAB function in Matlab/SIMULINK to calculate V_d, V_q, V_{ref} and angle α

3.5.2 Determination of Time Duration T_0, T_1 and T_2

The procedures for determining the switching time T_0, T_1 and T_2 is illustrated as follows (Tej & Ruchi, 2014).

Consider the sector 1 of the space vector hexagonal diagram in Figure 3.7 (Naresh *et al.,* 2012). If the amplitude V_{ref} at an angle α from the a-axis, then the inverter must spend time in the bounding states of the sector and the zero space vector state (Naresh *et al.,* 2012). Let the inverter spend time T_1 duration of time in state (1 0 0), T_2 duration of time in state (1 1 0) and T_0 duration of time in the zero space vector state (Tej *et al.,* 2014).

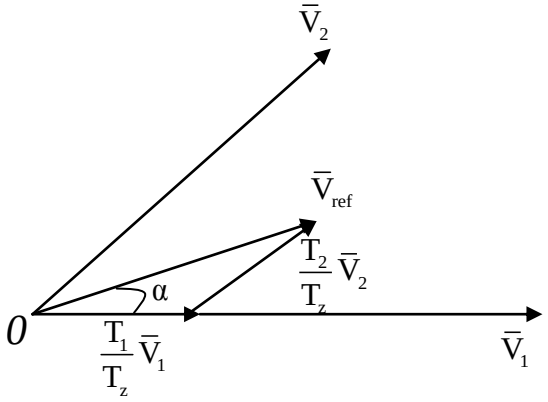


Figure 3.7: Reference Vector at Sector 1(Naresh *et al.,* 2012)

The switching duration of any sector is given as (Renu *et al.*, 2016; Rahul, 2014)

$$\int_0^{T_z} \bar{V}_{ref} = \int_0^{T_1} \bar{V}_1 dt + \int_{T_1}^{T_1+T_2} \bar{V}_2 dt + \int_{T_1+T_2}^{T_z} \bar{V}_0 dt \tag{3.31}$$

By integrating equation 3.31 from 0 to T_z, is therefore written as

$$T_z \bar{V}_{ref} = (T_1 \bar{V}_1 + T_2 \bar{V}_2) \tag{3.32}$$

From the Figure 3.7 $\bar{V}_{ref}$, $\bar{V}_1$ and $\bar{V}_2$ are expressed as

$$\bar{V}_{ref} = |\bar{V}_{ref}| \begin{bmatrix} \cos\alpha \\ \sin\alpha \end{bmatrix} \tag{3.33}$$

$$\bar{V}_1 = \frac{2}{3} V_{dc} \begin{bmatrix} 1 \\ 0 \end{bmatrix} \tag{3.34}$$

$$\bar{V}_2 = \frac{2}{3} V_{dc} \begin{bmatrix} \cos\frac{\pi}{3} \\ \sin\frac{\pi}{3} \end{bmatrix} \tag{3.35}$$

$\bar{V}_{ref}$, $\bar{V}_1$ and $\bar{V}_2$ was substituted into equation 3.32 as

$$T_z |\bar{V}_{ref}| \begin{bmatrix} \cos\alpha \\ \sin\alpha \end{bmatrix} = T_1 \frac{2}{3} V_{dc} \begin{bmatrix} 1 \\ 0 \end{bmatrix} + T_2 \frac{2}{3} V_{dc} \begin{bmatrix} \cos\frac{\pi}{3} \\ \sin\frac{\pi}{3} \end{bmatrix} \tag{3.36}$$

Where,

$$0 \leq \alpha \leq 60$$

Therefore, T_1, T_2 and T_0 are as

$$T_1 = T_z a \frac{\sin(\frac{\pi}{3} - \alpha)}{\sin(\frac{\pi}{3})} \tag{3.37}$$

$$T_2 = T_z a \frac{\sin(\alpha)}{\sin(\frac{\pi}{3})} \tag{3.38}$$

$$T_0 = T_z - (T_1 + T_2) \tag{3.39}$$

Where,

$T_z = \frac{1}{f_z}$, T_z is total time duration (3.40)

$a = \frac{|V_{ref}|}{2/3 V_{dc}}$, is modulation index (3.41)

The switching time duration at any sector is therefore written as

$$T_1 = \frac{\sqrt{3} T_z |\bar{V}_{ref}|}{V_{dc}} (\sin \frac{n}{3}\pi \cos\alpha - \cos \frac{n}{3}\pi \sin\alpha) \tag{3.42}$$

$$T_2 = \frac{\sqrt{3} T_z |\bar{V}_{ref}|}{V_{dc}} (\sin(\alpha - \frac{n-1}{3}\pi)) \tag{3.43}$$

$$T_0 = T_z - T_1 - T_2 \tag{3.44}$$

Where,

n = 1 (i.e. sector 1 -6) $0 \le \alpha \le 60$

Equations 3.42, 3.43 and 3.44 were written as algorithm in MATLAB function in Matlab/Simulink for sector identification and to calculate T_1, T_2 and T_0.

3.6 Determination of Switching Time of Each Transistor (S_1–S_6)

The switching pattern of each transistor (S_1–S_6) of the voltage source inverter is therefore configured as shown in Figure 3.8 (Dev, 2015).

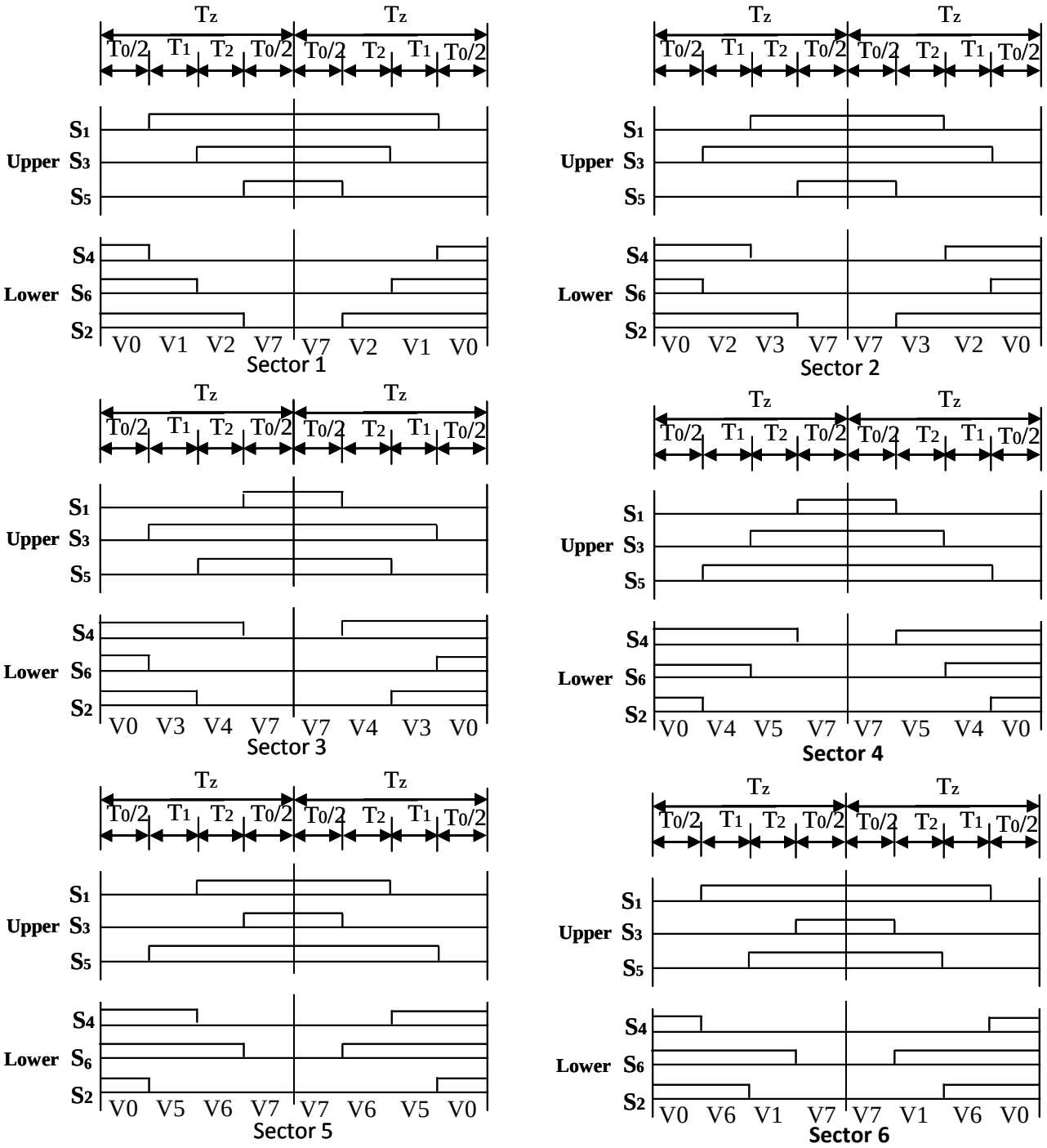


Figure 3.8: Space Vector PWM Switching Patterns at each Sector (Dev, 2015)

The switching time at each sector is summarized in Table 3.2 based on Figure 3.7, and it was written as algorithm in MATLAB function in MATLAB/SIMULINK to implement the switching time of each sector (Dev, 2015).

Table 3.2: Switching Time Calculation at Each Sector

Sector	Upper Switches (S1, S3, S5)	Lower Switches (S4, S6, S2)
1	S1 = T1 + T2 + T0/2 S3 = T2 + T0/2 S5 = T0/2	S4= T0/2 S6 = T1 + T0/2 S1 = T1 + T2 + T0/2
2	S1 = T1 + T0/2 S3 = T1 + T2 + T0/2 S5 = T0/2	S4= T2 + T0/2 S6 = T0/2 S1 = T1 + T2 + T0/2
3	S1 = T0/2 S3 = T1 + T2 + T0/2 S5 = T2 + T0/2	S4= T1 + T2 +T0/2 S6 = T0/2 S1 = T1 + T0/2
4	S1 = T0/2 S3 = T1 +T0/2 S5 = T1 +T2 + T0/2	S4= T1 + T2 + T0/2 S6 = T2 + T0/2 S1 = T0/2
5	S1 = T2 + T0/2 S3 = T0/2 S5 = T1 + T2 + T0/2	S4= T1 + T0/2 S6 = T1 +T2 + T0/2 S1 = T0/2
6	S1 = T2 + T0/2 S3 = T0/2 S5 = T1 + T0/2	S4= T0/2 S6 = T1 +T2 + T0/2 S1 = T2 + T0/2

Figure 3.9 show the flow chart of implementation of space vector pulse width modulation techniques in MATLAB/SIMULINK.

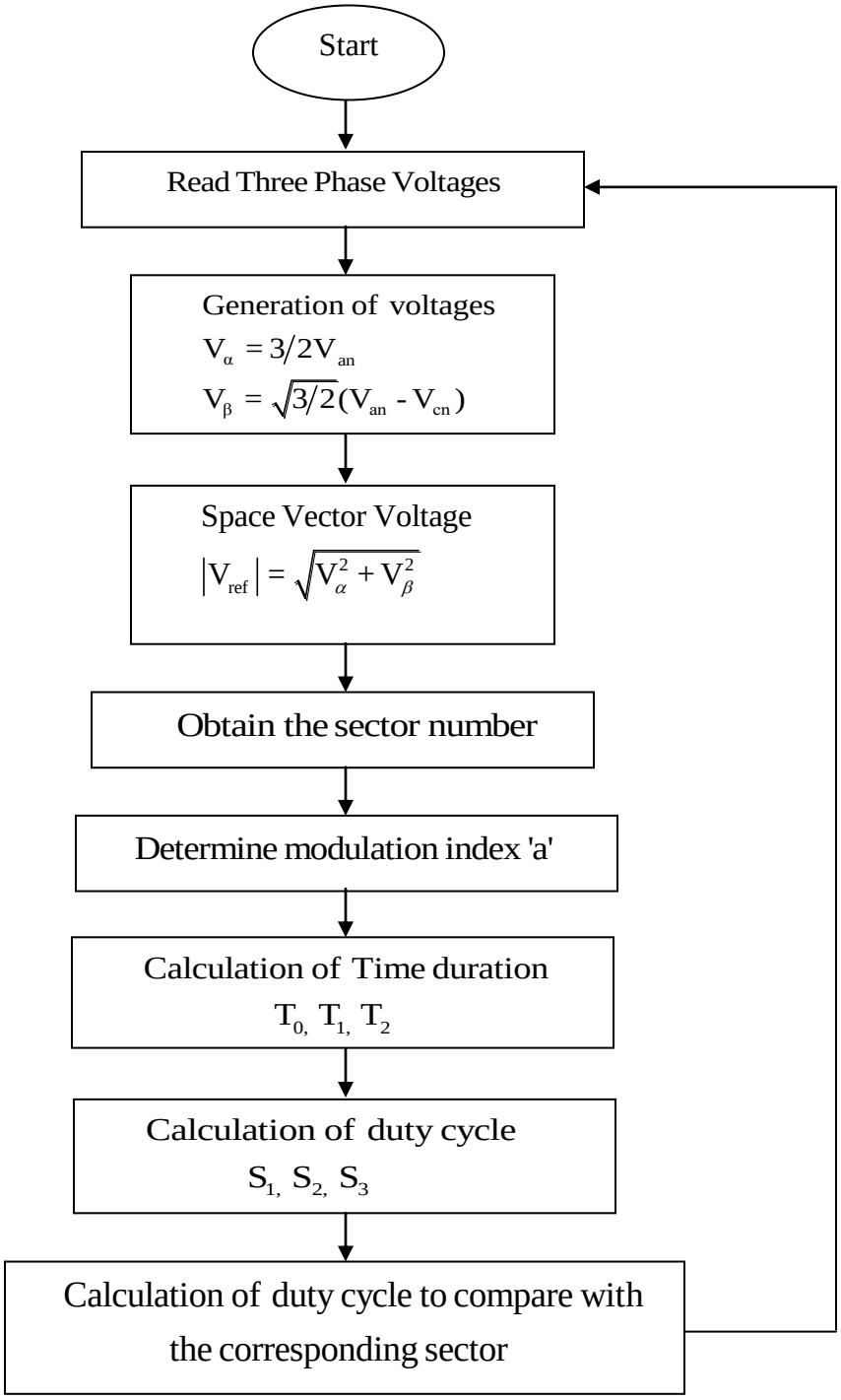


Figure 3.9: Flow chart for SVPWM implementation (Asma & Sayed, 2017).

The switching block diagram of space vector pulse width modulation techniques for generation of pulse signal for three phase inverter is shown in Figure 3.10

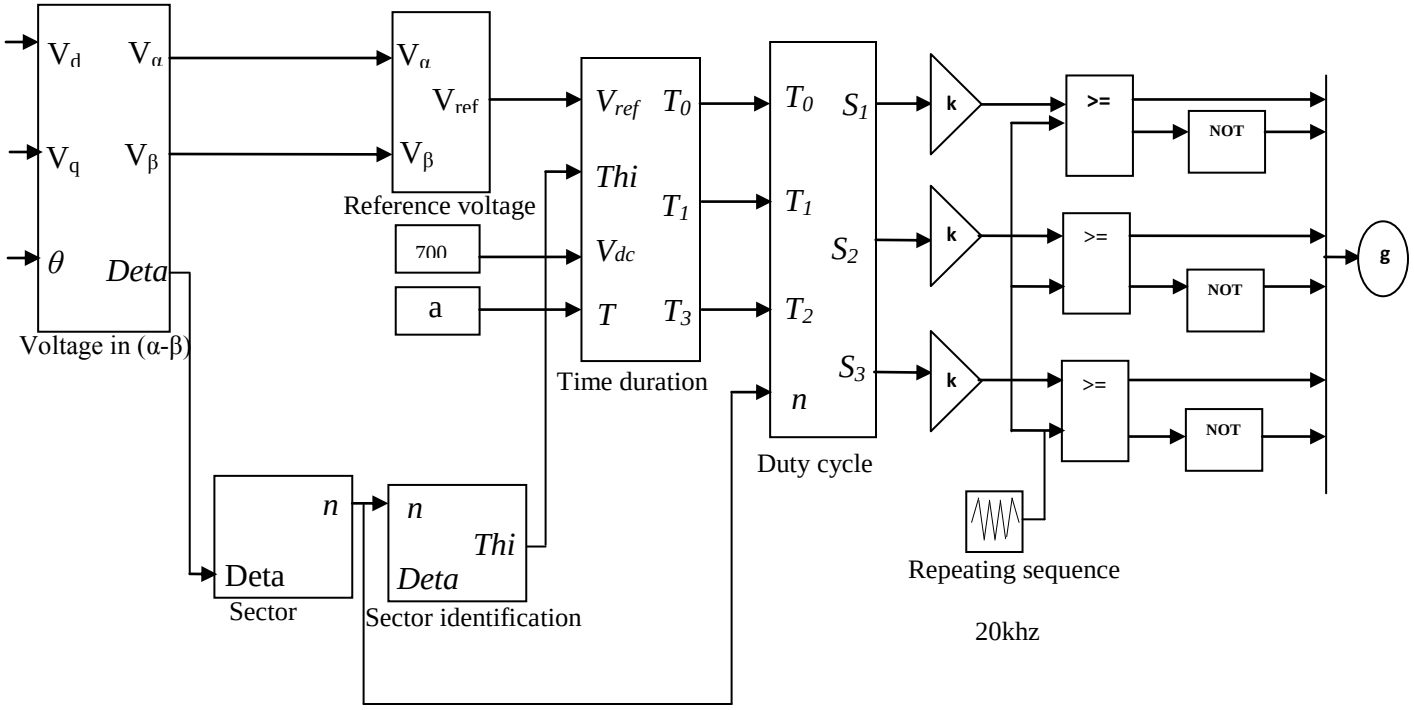


Figure 3.10: SVPWM based current control scheme for generating switching pulses (Subhransu & Siddharth, 2016).

CHAPTER FOUR
RESULTS AND DISCUSSION

4.1 Introduction

The results of simulations are detailed in this chapter. The harmonic analysis was done using Fast Fourier Transform (FFT) in MATLAB/SIMULINK environment as stated in methodology of this work. The performance of the developed SAPF model with space vector pulse width modulation was tested under balanced and unbalanced sinusoidal voltage source. The result obtained was compared with IEEE harmonic standard limit (< 5% THD). The work of Suleiman *et al.*, (2017) was used for validation.

4.2 Output Waveform of SVPWM with SAPF

The developed SVPWM model was simulated in Matlab/Simulink to compute the duty cycle of the three phase inverter switches and switching time duration of each sector. The three phase inverter is controlled by six switches configurations. In each configuration the vector identification uses a '0' to represent the negative phase voltage level and a '1' to represent the positive phase voltage level. The inverter voltage is "1" if the switch is on and "0" if it is off. The carrier signal with voltage amplitude of 1 and carrier frequency of 20 KHz was compared with reference signal. The output switching signal waveform is shown in Figure 4.1

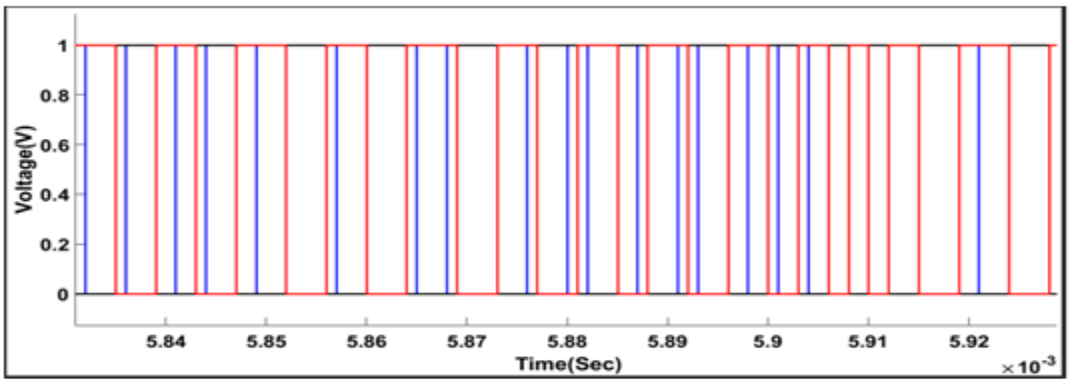


Figure 4.1: Output Switching Pulse of SVPWM at 20 KHz

4.3 SAPF with Balanced Voltage

The developed SAPF model was tested under balanced voltage before compensation and after compensation using SVPWM for RL and RC load. The result of SVPWM was compared with IEEE harmonic standard limit of 5% and Suleiman *et al.,* (2017) for validation.

4.3.1 Waveform of RL Load before Compensation

Figure 4.2 shows the waveforms of the source voltage and source current before compensation. The waveform of the simulation shows that source current is distorted and not in phase with source voltage due to the harmonic current generated by the RL load. The waveform shows that both fundamental and harmonics component are present in source current. This will increase the power loss as a result of poor power factor.

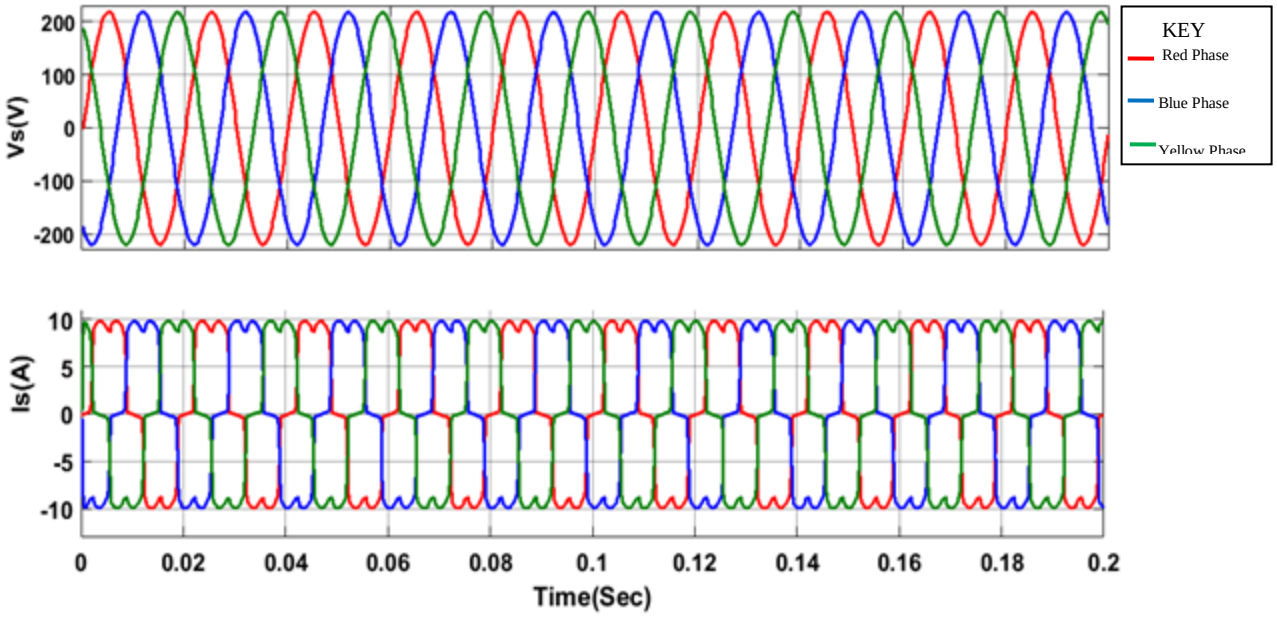


Figure 4.2: Waveforms of RL Load: Source Voltage (Vs) and Source Current (Is) before Compensation

4.3.2 Waveform of RL Load after Compensation with SVPWM

The developed SAPF model was tested with RL balanced load condition. Figures 4.3 shows the simulation waveforms of Source Voltage (Vs), Source Current (Is), Compensation Current (Ic) and DC Bus Voltage (V_{dc}). The results show that, the source current (*Is*) is now sinusoidal and in phase with the source voltage (*Vs*) when compared with the waveform in Figure 4.2. The result also shows the output waveform of SAPF (i.e. compensation current, *Ic*) injected at the PCC in equal opposite direction to cancel the harmonics present in the load current. The reference DC bus voltage was maintained constant at 700V using PI controller for effective performance of SAPF in harmonics mitigation. The initial delay time of the developed mode is 0.067s.

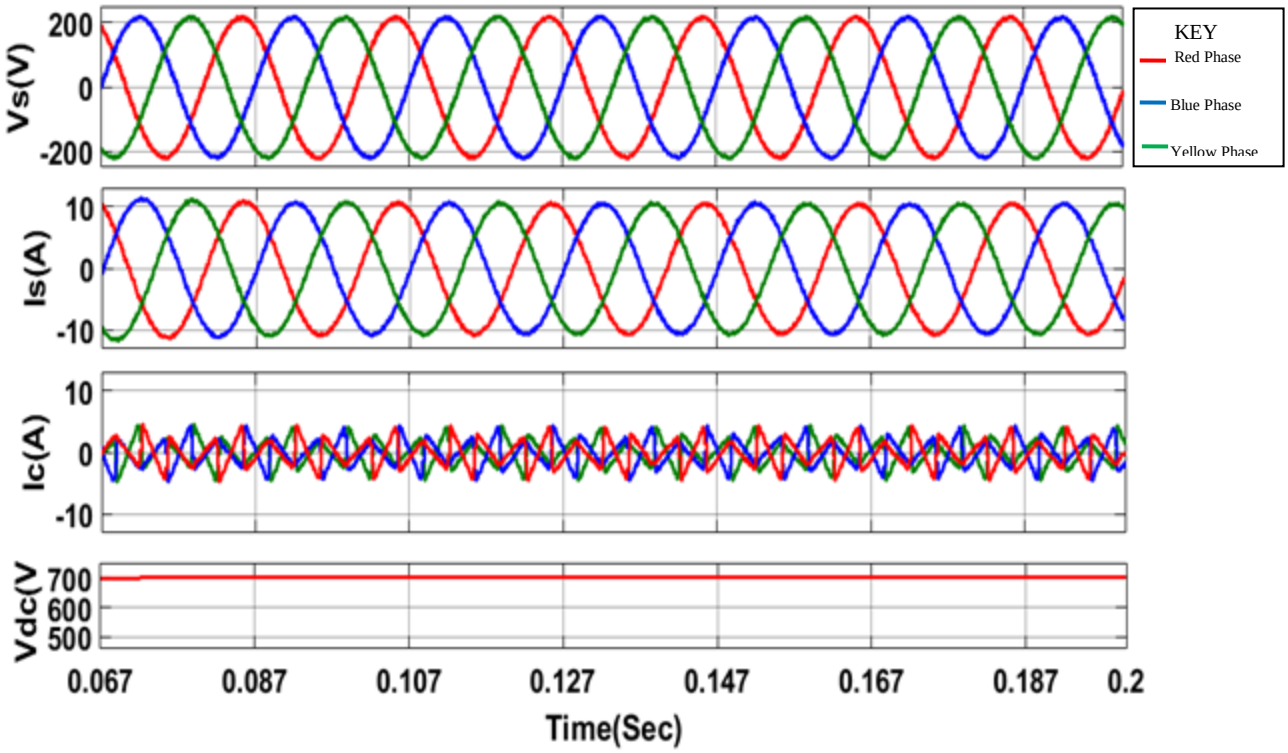


Figure 4.3: Simulation Waveform of RL Load with SVPWM: Source Voltage (Vs), Source Current (Is) after Compensation, Compensation Current (Ic) and DC Bus Voltage (V_{dc}).

4.3.3 Result of FFT Analysis of RL Load before Compensation

Figure 4.4 shows the Fast Fourier Transformation (FFT) of source current before compensation. The THD obtained is 25.60 % and the fundamental value of current at 50 Hz is 10.4 A. This THD value is large when compared with the IEEE standard harmonic limit (i.e < 5%). This is due to harmonics present in load current. Therefore, SAPF was applied to reduce the harmonics present in load current.

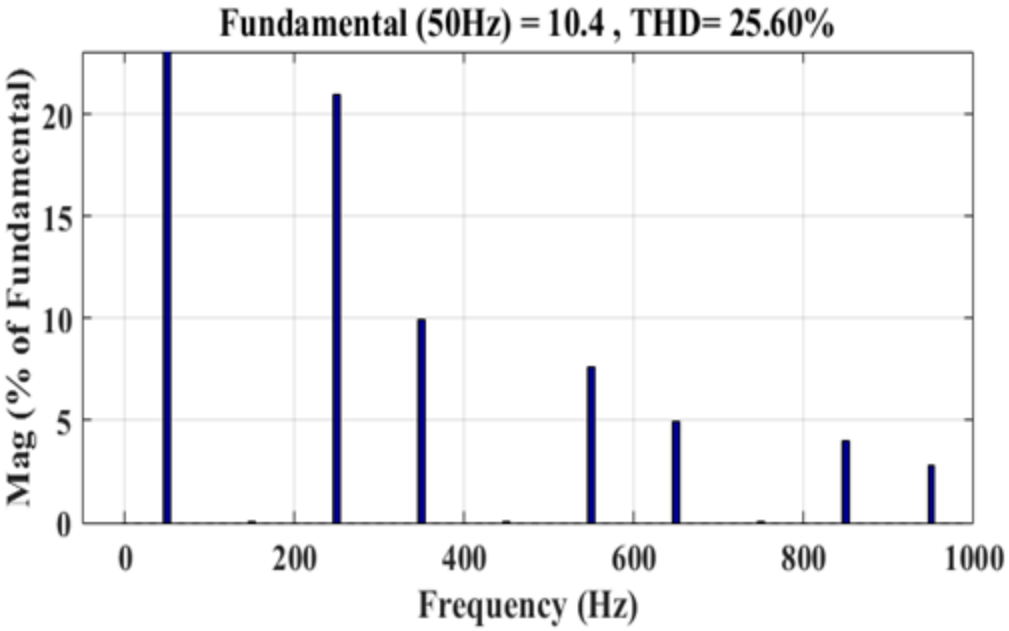


Figure 4.4: FFT of Source Current (Is) with RL Load before Compensation

4.3.4 Result of FFT Analysis of RL Load after Compensation with SVPWM

The developed SAPF model was subjected to Fast Fourier Transformation (FFT) analysis under balanced voltage with SVPWM. The result obtained in Figure 4.5 shows the Fast Fourier Transformation (FFT) analysis of source current after compensation. The result shows a significant Total Harmonic Distortion reduction from 25.6% to 0.91% as seen in Figure 4.4. The result is within the range of IEEE harmonic standard limit of 5%.

The result shows that SVPWM has performed better than fuzzy logic controller as developed by Suleiman *et al.*, (2017) which is 0.92% in term of harmonic reduction.

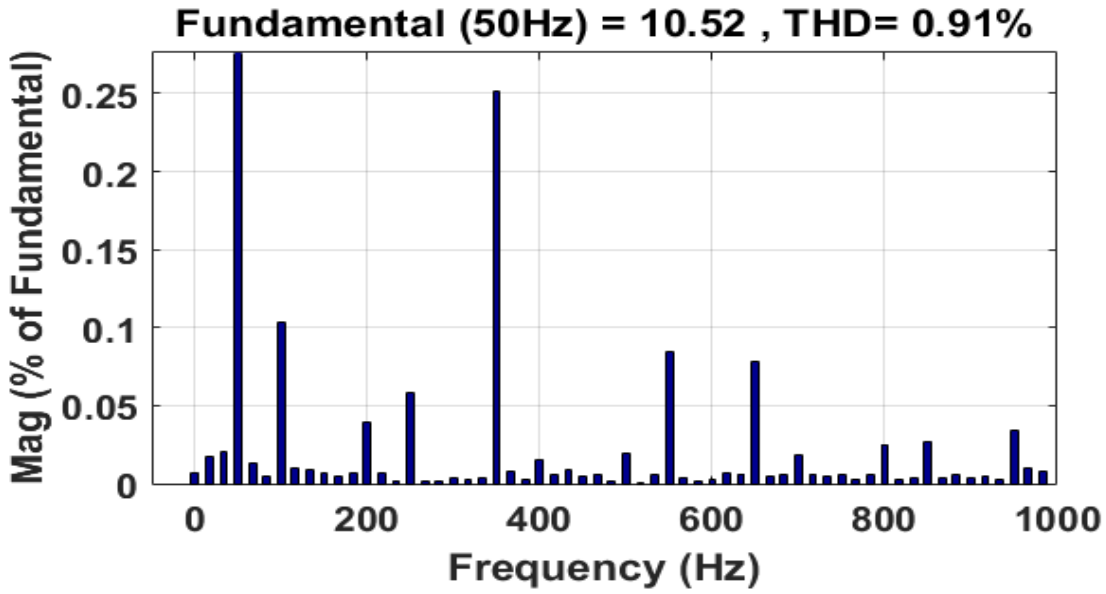


Figure 4.5: FFT of the Source Current (I_S) after Compensation with SVPWM for RL Load

4.3.5 Waveform of RC Load before Compensation

The SAPF model was subjected to RC load with load capacitance of 2200μF and load resistance of 20Ω (Suleiman *et al.,* 2017). Figure 4.6 shows the waveforms of the source voltage and source current before compensation. The waveform of the simulation shows that source current is not sinusoidal and not in phase with the source voltage due to the harmonic current generated by the RC load. The waveform shows that both fundamental and harmonics component are present. This will increase the power loss (i^2R) as a result of poor power factor (Suleiman *et al.,* 2017).

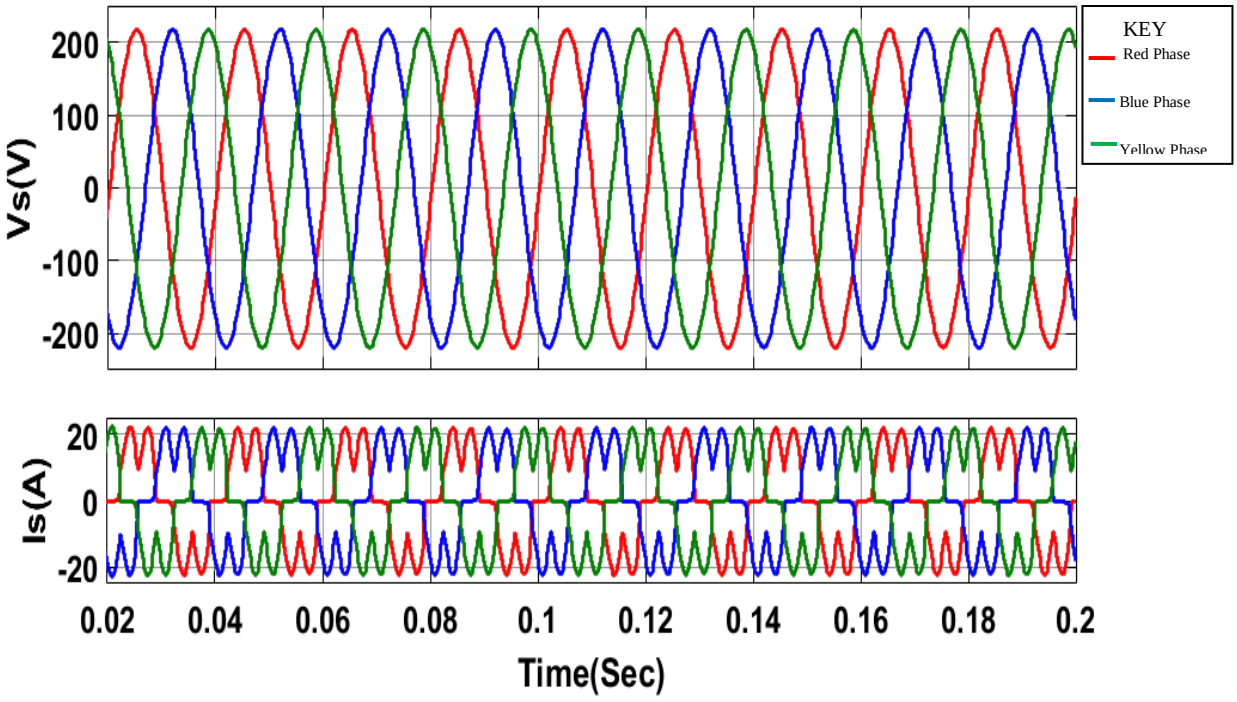


Figure 4.6: Waveforms of RC Load: Source Voltage (Vs), Source Current before Compensation

4.3.6 Waveform of RC Load after Compensation with SVPWM

The developed SAPF model was tested with RC balanced load condition. Figure 4.7 shows the simulation waveforms of Source Voltage (Vs), Source Current (Is), Compensation Current (Ic) and DC Bus Voltage (V_{dc}). The results show that, the Waveform of the source current (*Is*) is now sinusoidal and in phase with the source voltage (*Vs*) when compared with the waveform in

Figure 4.6. The waveform also shows compensation current (*Ic*) for harmonic cancellation at the PCC and the DC bus voltage (*Vdc*). The reference DC bus voltage was maintained constant at 700V using PI controller for effective performance of SAPF. The initial delay time of the developed model is 0.09s

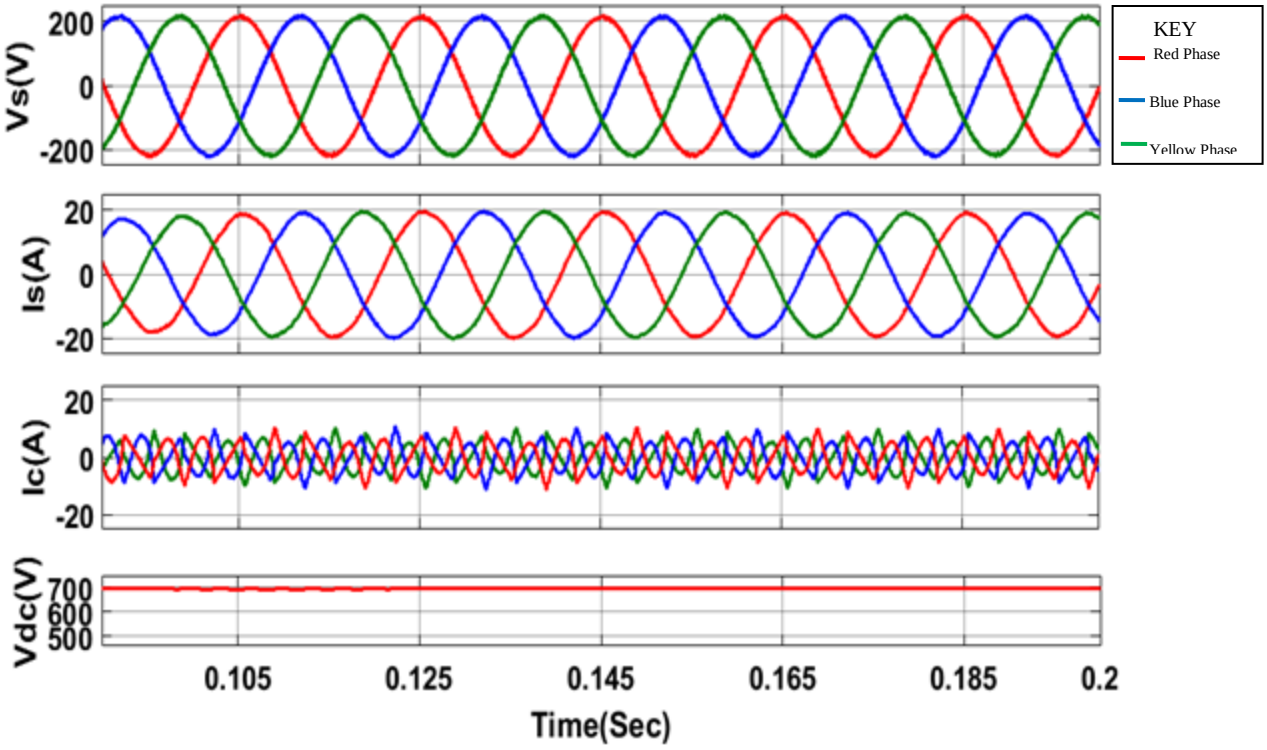


Figure 4.7: Simulation Waveform of RC Load with SVPWM: source voltage (Vs), Source current (Is) after compensation, Compensation current (Ic), and DC bus voltage (V_{dc}).

4.3.7 Result of FFT Analysis of RC Load before Compensation

Figure 4.8 shows the Fast Fourier Transformation (FFT) analysis of Source current before compensation. The THD obtained is 35.46 % and the fundamental value of current at 50Hz is 18.87 A. This THD value is large when compared with the IEEE standard. This is due to the harmonics present in the load current. Therefore, SAPF was applied by injecting compensating current at the PCC to reduce the value of harmonics present in the load current.

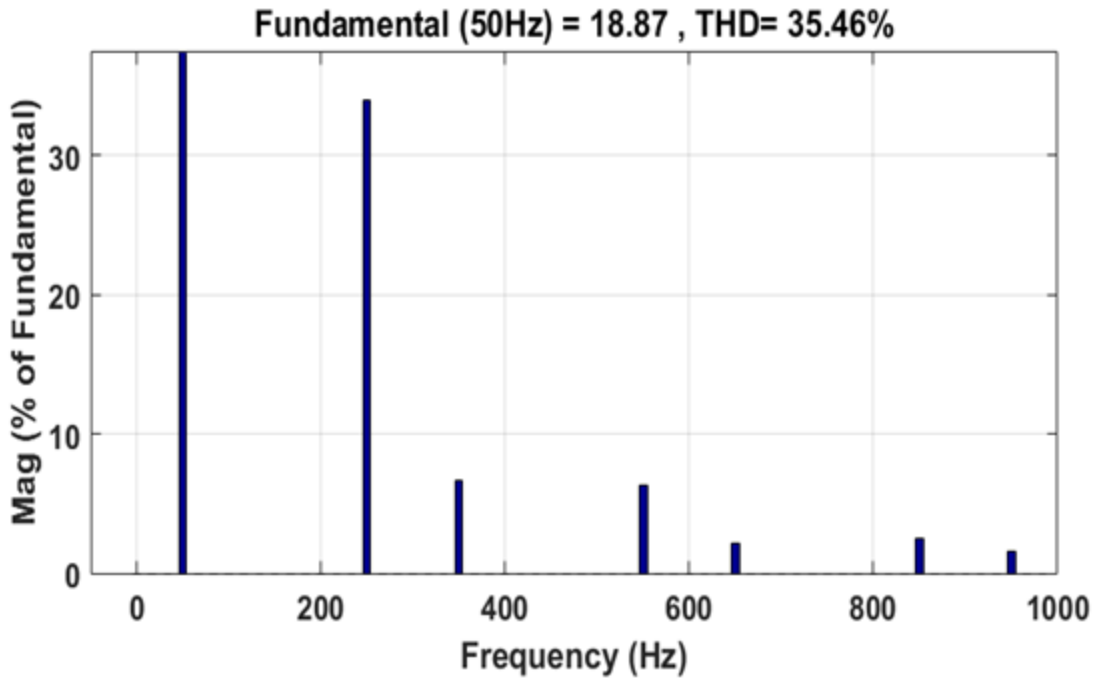


Figure 4.8: FFT of Source Current (I_S) with RC Load before Compensation

4.3.8 Result of FFT Analysis of RC Load after Compensation with SVPWM

The developed SAPF model was subjected to Fast Fourier Transformation (FFT) analysis under balanced voltage with SVPWM. The result obtained in Figure 4.9 shows the Fast Fourier Transformation (FFT) analysis of Source current after compensation. The result shows a significant reduction of Total Harmonic Distortion from 35.46% to 1.35% as seen in Figure 4.9.

The result is within the range of IEEE harmonic standard limit of 5%. The fundamental current value was also increased from 18.87A to 19.21A.

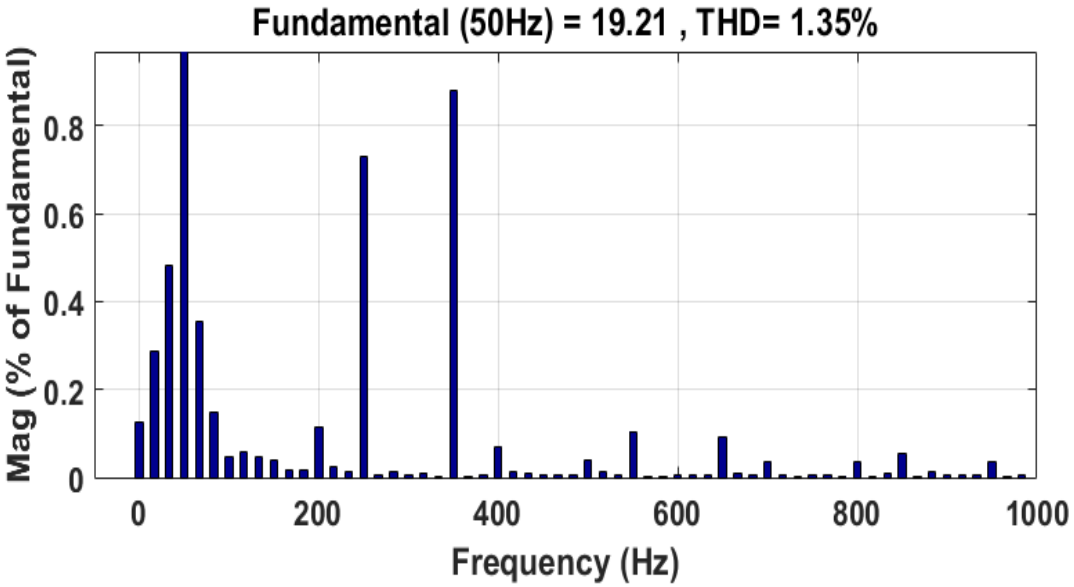


Figure 4.9: FFT of Source Current (I_S) after Compensation with SVPWM for RC load

Table 4.1 Summary of Results of Balanced Voltage System with SAPF

Load	Control Strategy	THD without SAPF	THDs (%) with SAPF	
			SVPWM	FLCPWM
RL	MSRF	25.60	0.91	0.92
RC	SRF	35.46	1.35	-

4.4 SAPF with Unbalanced Voltage

The performance of developed SAPF model was also tested under unbalanced voltage before compensation and after compensation using SVPWM for RL and RC load. The performance of SVPWM was compared with IEEE harmonic standard limit of 5%. The National Electrical Manufacturers Association (NEMA) standard (1993) defines percentage unbalance voltage as the ratio of maximum voltage deviation from average value to the average voltage. They recommended that the percentage voltage unbalance should not exceed 1% at motor terminal.

4.4.1 Waveform of RL Load before compensation

The developed SAPF model was tested with unbalanced source voltage of $V_A = 200V$, $V_B = 210V$, $V_C = 220V$. Figure 4.10 shows the waveforms of the source voltage and source current before compensation. The waveform of the simulation shows that source current is highly distorted and not sinusoidal due to the harmonic current generated by the combination of RL load and unbalanced voltage. The waveform shows that both fundamental and harmonics component are present. This will increase the power loss as a result of poor power factor.

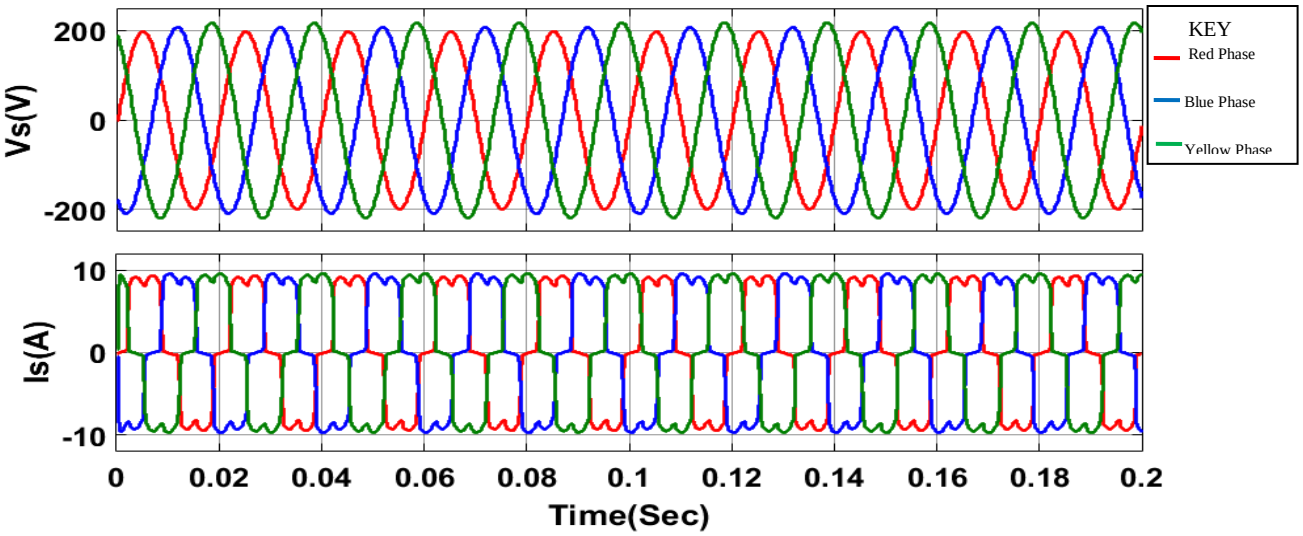


Figure 4.10: Waveforms of RL Load Under Unbalanced Voltage: Source Voltage (Vs), Source Current before Compensation

4.4.2 Waveform of RL Load after Compensation with SVPWM

The developed SAPF model was tested with RL balanced load condition. Figures 4.11 shows simulation waveforms of Source Voltage (Vs), Source Current (Is), Compensation Current (Ic) and DC Bus Voltage (V_{dc}). The results show that, the source current (*Is*) is now sinusoidal and in phase with the source voltage (*Vs*) when compared with Figure 4.10. The result also shows the waveform of compensation current (*Ic*) injected at the PCC in equal opposite direction to cancel the harmonics present in the load current and the DC bus voltage (*Vdc*). The reference DC bus voltage was maintained constant at 700V using PI controller for effective performance of SAPF in harmonics mitigation. The initial delay time of the developed model is 0.067s

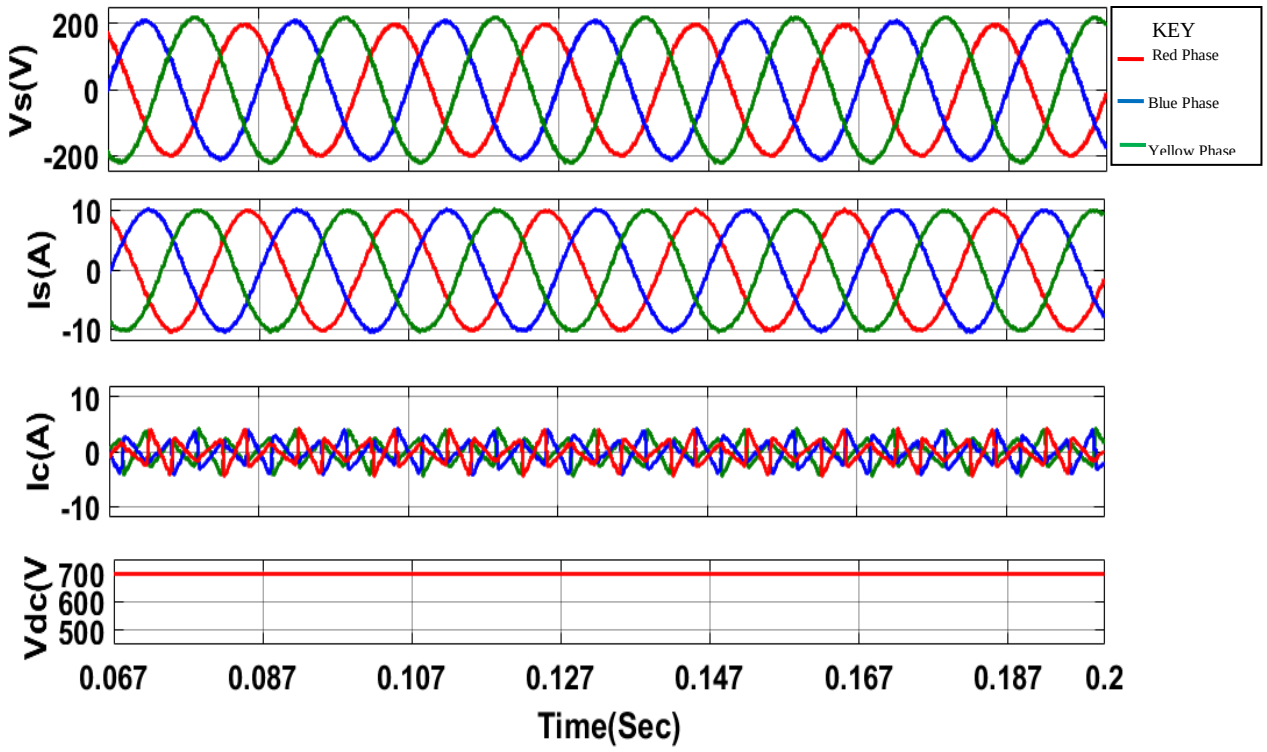


Figure 4.11: Simulation Waveform of RC Load with SVPWM: source voltage (Vs), Source current (Is) after compensation, Compensation current (Ic), and DC bus voltage (V_{dc}).

4.4.3 Result of FFT Analysis of RL Load Prior to Compensation

Figure 4.12 shows the Fast Fourier Transformation (FFT) analysis of Source current before compensation. The THD obtained is 26.68 % and the fundamental value of current is 9.701 A. This THD value is large when compared with the IEEE standard harmonic limit (i.e < 5%). This is due to harmonics present load current. Therefore, SAPF was applied to reduce the harmonics present in load current.

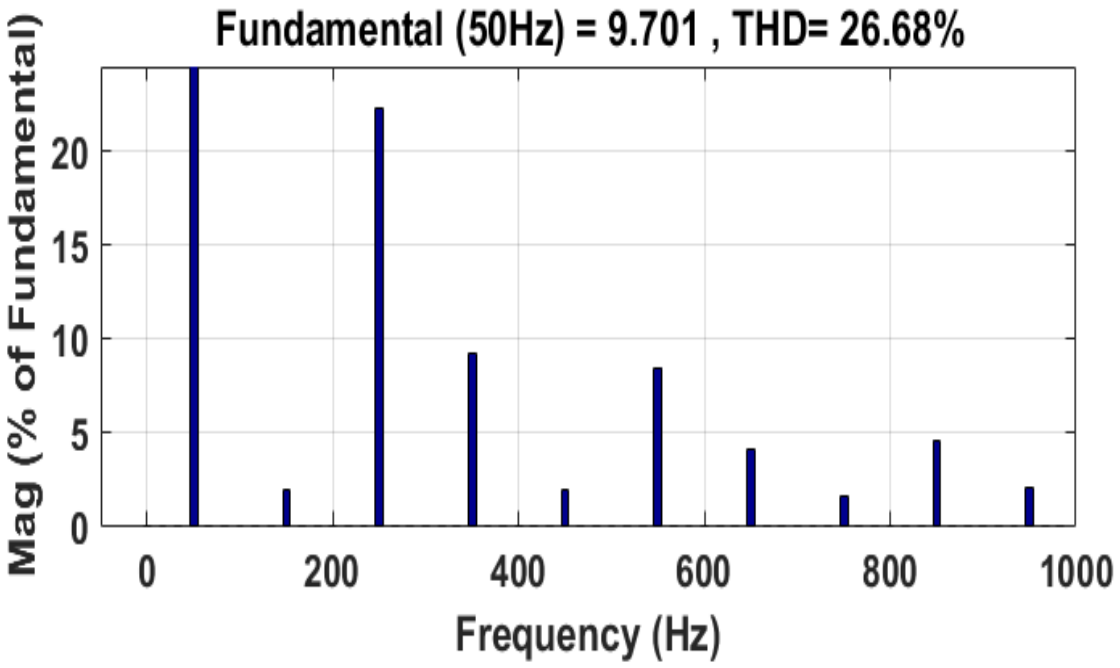


Figure 4.12: FFT of Source Current (I_S) with RL Load before Compensation

4.4.4 Result of FFT Analysis of RL Load after Compensation with SVPWM

The developed SAPF model was subjected to Fast Fourier Transformation (FFT) analysis under balanced voltage with SVPWM. The result obtained in Figure 4.13 shows the Fast Fourier Transformation (FFT) analysis of Source current after compensation. The result shows a significant 1.74% reduction of THD when compared with 26.80% in Figure 4.12. The result is

within the range of IEEE harmonic standard limit of 5%. The fundamental current value has increased from 9.701A to 9.938A.

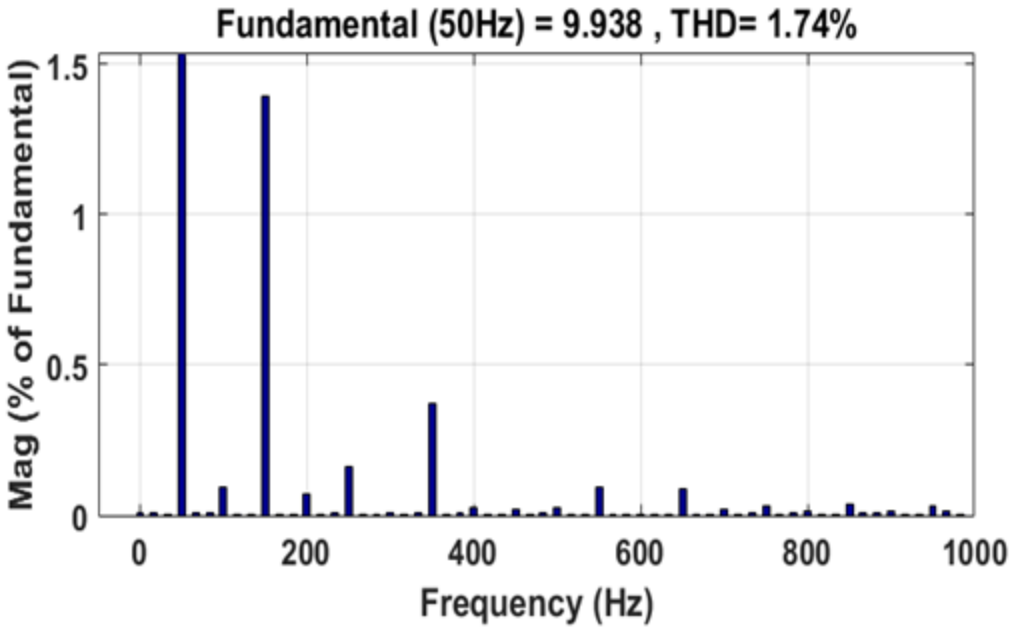


Figure 4.13: FFT of the Source Current (I_S) after Compensation with SVPWM for RL Load

4.4.5 Waveform of RC Load before Compensation

The SAPF model was subjected to RC load with load capacitance of 2200μF and load resistance 20Ω (Suleiman, 2017). Figure 4.14 shows waveforms of the source voltage and source current before compensation. The waveform of the simulation shows that source current is not sinusoidal and not in phase with the source voltage due to the harmonic current generated by the RC load. The waveform shows that both fundamental and harmonics component are present. This will increase the power loss (i^2R) as a result of poor power factor (Suleiman *et al.*, 2017).

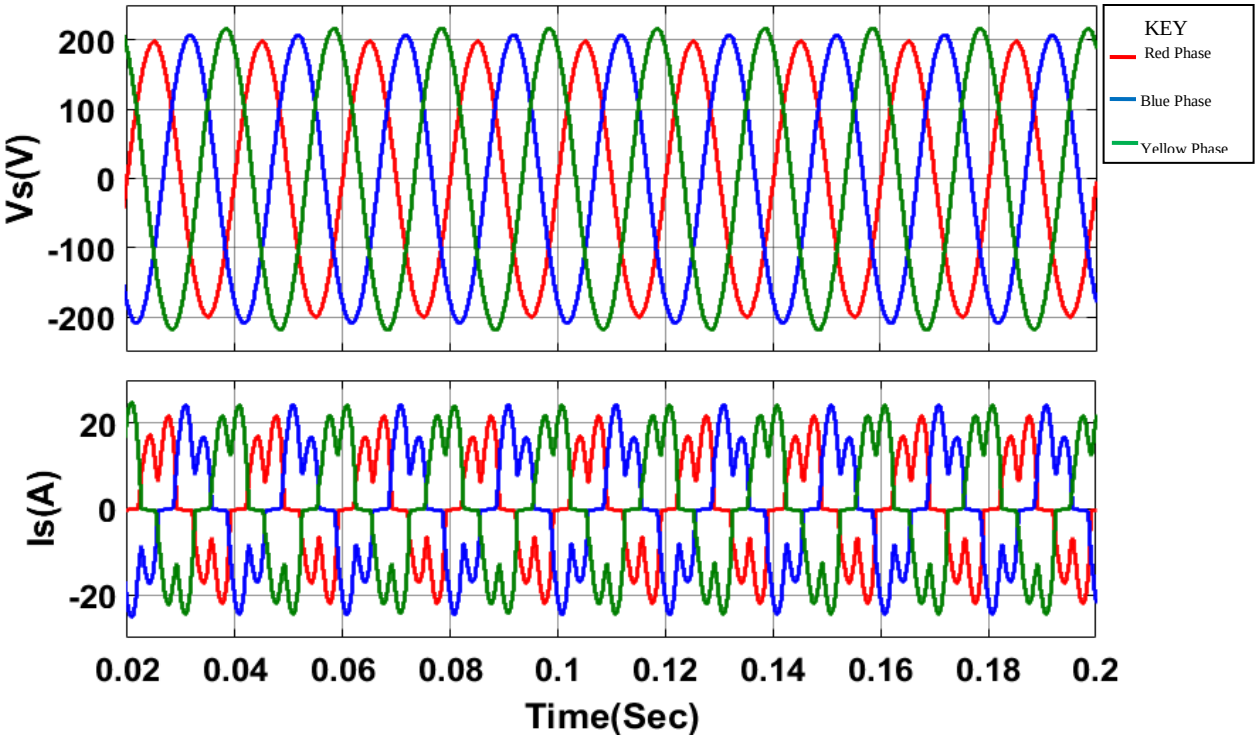


Figure 4.14: Waveforms of RC Load: Source Voltage (Vs), Source Current before Compensation

4.4.6 Waveform of RC Load after Compensation with SVPWM

The developed SAPF model was tested with RC unbalanced load condition. Figures 4.15 shows simulation waveforms of Source Voltage (Vs), Source Current (Is), Compensation Current (Ic) and DC Bus Voltage (V_{dc}). The results show that, the Waveform of the source current (*Is*) is now sinusoidal and in phase with the source voltage (*Vs*) when compared with Figure 4.14. The result

also shows the output waveform of SAPF (i.e. compensation current, *Ic*) and the DC bus voltage (*Vdc*). The reference DC bus voltage was maintained constant at 700V using PI controller for effective performance of SAPF. The initial delay time of the developed model is 0.095s

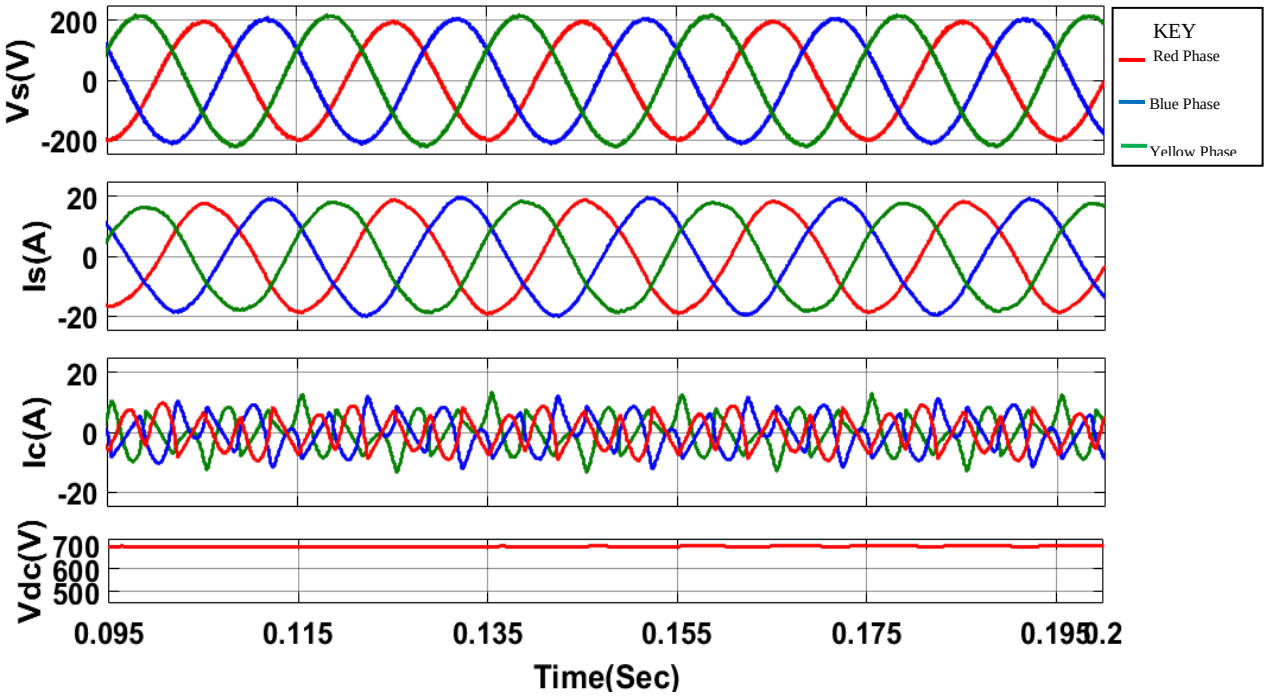


Figure 4.15: Waveform of RC Load with SVPWM: source voltage (Vs), Source current (Is) after compensation, Compensation current (Ic), and DC bus voltage (V_{dc}).

4.4.7 Result of FFT Analysis of RC Load before Compensation

Figure 4.16 shows the Fast Fourier Transformation (FFT) analysis of Source current before compensation. The THD obtained is 41.83 % and the fundamental value of current is 16.09 A. This THD value is large when compared with the IEEE standard. This is due to the harmonics present in the load current. Therefore, SAPF was applied by injecting compensating current at the PCC to reduce the value of harmonics present in the load current.

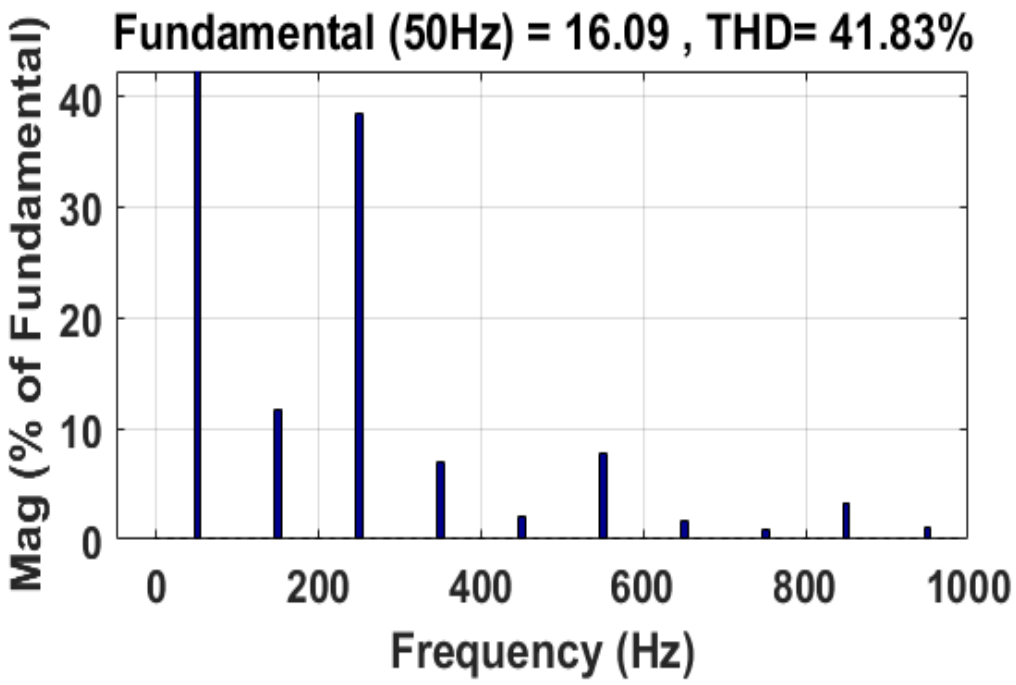


Figure 4.16: FFT of Source Current (I_S) before Compensation with RC Load

4.4.8 Result of FFT Analysis of RC Load after Compensation with SVPWM

The developed SAPF model was subjected to Fast Fourier Transformation (FFT) analysis under balanced voltage with SVPWM. The result obtained in Figure 4.17 shows the Fast Fourier Transformation (FFT) analysis of Source current after compensation. The result shows a significant reduction of Total Harmonic Distortion from 41.83% to 3.01% as seen in Figure 4.16.

The result is within the range of IEEE harmonic standard limit of 5%. The fundamental current value was also increased from 18.25A to 16.09A. See Table 4.2 for summary of the results

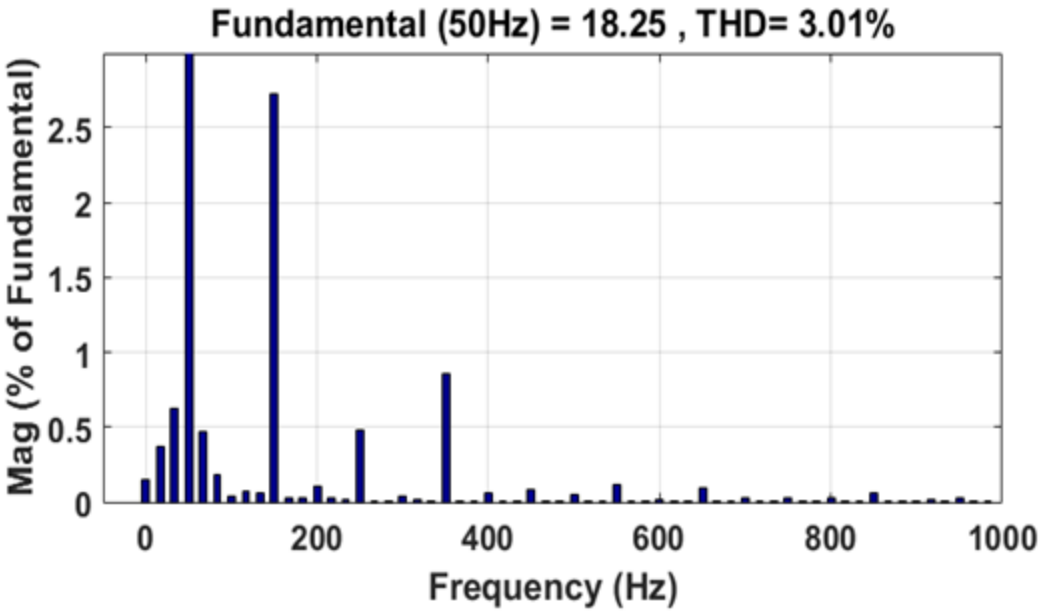


Figure 4.17: FFT of Source Current (I_S) after Compensation with SVPWM for RC Load

Table 4.2: Summary of Results of Balanced Voltage System with SAPF

Load	Control Strategy	THD without SAPF	THDs (%) with SAPF SVPWM
RL	SRF	26.68	1.74
RC	SRF	41.83	3.01

CHAPTER FIVE

CONCLUSION AND RECOMMENDATION

5.1 Conclusion

Shunt Active Power Filter (SAPF) with Space Vector Pulse Width Modulation (SVPWM) based current control method has been developed for harmonic reduction. Synchronous reference frame theory was used to transform ac in a-b-c quantities into DC in d-q quantities and also as control strategy to extract reference harmonic current. The developed model was tested for both RL and RC load under balanced and unbalanced sinusoidal voltage. FFT analysis shows that harmonic has been reduction from 25.60 % to 0.91 % (THD) for RL nonlinear load. The result shows an improvement of 1.087% when compared with the work of Suleiman *et al.,* 2017 using FLCPWM with the result of 0.92% (THD). FFT analysis shows that all the results are within the limit of IEEE 519 standard.

5.2 Limitation

The developed SVPWM model was tested with balanced loads condition. It was not tested with unbalanced loads condition.

5.3 Significant Contribution

The following are some of the significant contributions from the research work

1. A SAPF was developed for harmonic reduction using SVPWM as a current controller for switching pulse signal generation.

2. SVPWM was tested under balanced sinusoidal voltage using RL non linear load and a harmonic reduction of 0.91% THD was achieved as compared to 0.92% THD of the work of Suleiman et al., (2017). This shows an improvement of 1.087%.

3. SVPWM was also tested under unbalanced sinusoidal input voltage using RL load and a significant harmonic reduction of 1.74% THD after compensation was achieved as compared to 26.68% THD before compensation.

5.4 Recommendation

The following are recommended as future works that can be considered:

i. Intelligent controller can be used to replace PI controller to maintain the DC bus voltage constant during the transient period.

ii. This work can be implemented on hardware to validate the performance of shunt active power filter.

REFERENCES

Abdeldjabbar, M. K. & Tayeb, A. (2017). Adaptive Hysteresis Band Based Fuzzy Controlled Shunt Active Power Filter. *Paper Presented at International Symposium on Industrial Engineering and Operations Management (IEOM), Bristol, U.K., IEEE Conference,* 718-726.

Abhijit, A. I. and Kompelli, S. (2016). Harmonics Reduction With Id-Id Control Strategy Using Fuzzy Logic Controller Based Three-Phase Shunt Active Power Filter (SAPF). *International Journal of Research Publications in Engineering and Technology,* (2)5, 10-15.

Akash, K. C., Pushprajsinh, T. & Bipinkumar, T. & Bipinkumar, N. (2016). Simulation and Analysis of Shunt Active Power Filter (SAPF). *International Research Journal Of Engineering And Technology (IRJET),* (3)5, 1902-1906.

Akash, N. B. & Mukund, R. S. (2015). Performance Analysis of Active Power Filter (SAPF) With Different Switching Generation Techniques. *International Journal of Science and Research (IJSR),* (4)4, 331-336.

Asma & Sayed, B. H. (2017). Implementation of Different Methods of Space Vector Pulse Width Modulation- A survey. *International Journal for Innovative Research in Science and Technology,* (3)9, 73-81.

Ali, C., Mohammed, K. F., Mohamed, F. B. & Abdelhalim, K. (2015). Sliding Mode Control for Four Legs Shunt Active Power Filter (SAPF) to Eliminate Zero Sequence Current, Compensating Harmonics and Reactive Power with Fixed Switching Frequency. *Serbian Journal of Electrical Engineering,* (12)2, 205-218.

Balasubramaniam, P. M., Prabha, S. U., Chennai, T. N. & Sathyamangalam, T. N. (2014). A Practical Approach to Harmonics Compensation in Electrical Power Systems Using Shunt Active Power Filter (SAPF). *International Journal of Soft Computing,* 9(3), 160-168.

Bimal, K. B. (2006). Power Electronics Motor Drives. *Academic Press Publication, USA.*

Brahim, B. & Chellali, B. (2011). Power Quality Enhancement Using Shunt Active Power Filter (SAPF) Based on PSO. *Journal of Applied Sciences,* 11(22), 3725-3731.

Chelli, Z., Toufouti, R., Omeiri, A. & Saad, S. (2015). Hysteresis Control for Shunt Active Power Filter (SAPF) Under Unbalance and Three-Phase Load Condition. *Journal of Electrical and Computer Engineering,* 2015, 1-10.

Chennai, S. & Benchouia, M. T. (2011). Intelligents Controller for Shunt Active Power Filter (SAPF) to Compensate for Harmonics Based on SRF and SCR Control Strategies. *International Journal of Electrical Engineering and Informatics,* 3(3), 372-393.

Chennai, S. & Benchouia, M. T. (2014). Three-Phase Three-Level (NPC) Shunt Active Power Filter (SAPF) Performances Based on PWM and ANN Controllers for Harmonic Current

Compensation. *International Journal of Electrical Engineering and Informatics*, 6(2), 532-552.

Dev, K. T. (2015). Power Quality Improvement Using DVR. *M.Sc Thesis, Department of Electrical Engineering, National Institute of Technology, Rourkela*.

Emmanuel, W. (2012). Power Quality Disturbances in Production Facilities. *B.Sc Thesis, Chalmers University of Technology Gothenburg, Sweden.*

Fazard, S. M. & Mahid, S. (2014). The Effect of New Adaptive HCC for Shunt Active Power Filter (SAPF) in The Grid Connected Photovoltaic System. *International Research Journal of Applied and Basic Sciences*, 8 (1), 103-109.

Hemachandran, K., Nishanth, P., Justus, B. R. & Darly, S. S. (2015). Method of Improving Power Quality Using FPGA with SAPF in Power Systems. *SSRG International Journal of Electrical and Electronics Engineering (SSRG-IJEEE)*, 2(10), 8-10.

Hussein, M. E. F. (2012). Power Quality Assessment. *Ph.D Thesis, Faculty of Engineering Al-azhar University Cairo, Egypt.*

Irfan, A., Virendra, S. & Pradeep, C. (2016). Control Techniques for Active Power Filter for Harmonic Elimination and Power Quality Improvement. *International Journal of Electrical, Electronics and Data Communication*, 4, (10), 25-36.

Jin-Woo, J. (2005). Project Number Two Space Vector Pwm Inverter. *Ph.D Project, Mechatronic Systems Laboratory Department of Electrical And Computer Engineering. The Ohio State University.*

Kale, M. & Ozdemir, E. (2015). A new hysteresis band current control technique for a shunt active filter. *Turkish Journal of Electrical Engineering & Computer Sciences.* 23, 654 - 665.

Karupannan, P. (2012). Design and Implementation of Shunt Active Power Line Conditioner using Novel Control Strategies. *PhD Thesis, National Institute of Technology Rourkela-769 008 (ODISHA).*

Kumar, P. (2015). Harmonics Elimination and Power Factor Correction Using Space Vector Modulation (SVM). *Asian Journal of Current Engineering and Maths,* 4(6), 83-87.

Kumar, V. E., Arvind, A. B. & Nilesh, M. C. (2015). Self Tuning Filter Method for Real Time Control of Three-Phase Shunt Active Power Filter (SAPF). *International Journal of Engineering Researches and Management Studies*, 2(2), 1-6.

Laith, A. (2016). Shunt Active Power Filtering for Smart Appliances. *M.Sc Thesis, Department of Electrical & Computer Engineering of Mc Master University, Hamilton, Ontario, Canada.*

Manjulata, B. (2012). Power Quality Improvement Using Passive Shunt Filter, TCR and TSC Combination. *M.Sc Thesis*, National Institute of Technology, Rourkela, India.

Marwa, B. R., Mohamed W . N., Ilhem S. B., Eric, M. (2017). An Improved LCL Filter Design in Order to Ensure Stability without Damping and Despite Large Grid Impedance Variations. *Energies 2017 Article,* 10(336), 1-19.

Mernis, B. V. (2015). Active Power Filters for Nonlinear Load Applications. *M.Sc Thesis, Chalmers University of Technology Gothenburg, Sweden.*

Mohamed, A. M., Mahmoud, A. S., Essam, E. M. & Mohamed, M. H. (2017). Comparison of Shunt Active Power Filter Control Strategies for Harmonic Compensation in a Paper Industrial Factory. *American Journal of Management Science and Engineering,* 2(3), 41-51.

Mohammad, S. (1999). A Robust VSC-Based Shunt Active Power Filter. *Ph.D Thesis, University of Toronto.*

Mohammed, K. (2012). Investigation of Shunt Active Power Filter For Power Quality Improvement. *M.Sc Thesis, Near East University.*

Murat, K. & Engin, O. (2004). An Adaptive Hysteresis Band Current Controller for Shunt Active Power Filter. Elsevier, *Electric Power Systems Research* 73 (2005), 113–119.

Nalini C. K., Subhransu, S. D. & Prema, S. L (2011). A Few Aspects of Power Quality Improvement Using Shunt Active Power Filter. *International Journal of Scientific & Engineering Research,* 2(5), 1-11.

Naresh, K. & Prabhat, K. (2012). Hybrid Active Filter Based On SVPWM for Power Conditioning Using Matlab/Simulink Toolbox Environment. *International Journal of Electronic and Electrical Engineering,* 5(2), 113-133.

Niklesh, D. & Sandeep, M. (2017). Power Quality Improvement of Three-Phase System Using Shunt Active Power Filter (SAPF). *International Journal of Innovation Research in Electrical, Electronics, Instrumentation and Control Engineering,* 5(3), 23-26.

Phuong, H. T. (2012). Matlab/Simulink Implementation and Analysis of Three Pulse-Width-Modulation (PWM) Techniques. *M.Sc Thesis, Boise State University.*

Pradeep, K. D. (2007). Investigations on Shunt Active Power Filter for Power Quality Improvement. *M.Sc Thesis, Department of Electrical Engineering, National Institute of Technology, Rourkela.*

Prakash, C. T., Anup, K. P., Bibhu, P. P & Hari, N. P. (2016). A Comparative Performance Analysis of Id-Iq and Artificial Neural Network (ANN) Based Control Strategies for Current Harmonics Mitigation in Three-Phase Four-Wire System. *International Journal of Control Theory and Applications (IJCTA),* 9(14), 6903-6917.

Priyanka, S. S & Shruti, G. (2017). Implementation of shunt active power filter with comparative study of SPWM and SVPWM technique for reduction of THD. *International. Journal of Engineering Research and Application,* 7(9), 42-47.

Rahul, K. G. (2014). Implementation of Shunt Active Power Filter (SAPF) Algorithms. *B.Tech. Thesis, Department of Electrical Engineering, National Institute of Technology, Rourkela.*

Rama, M. G. & Sobharani, Y. (2014). Simulation and Analysis of Shunt Active Power Filter (SAPF) for Power Quality Improvement. *International Journal of Advance Trends in Computer Science and Engineering,* 3(1), 26-31.

Rama, R. P., Devikiran, P. & Saranya, M. D. (2016). Modeling and Analysis of Controller for Three-Phase Shunt Active Power Filter (SAPF). *International Journal of Signal Processing, Image Processing and Pattern Recognition,* 9(1), 103-110.

Rathika, P. & Devaraj, D. (2011). A Novel Fuzzy Adaptive Hysteresis Controller Based Three Phase Four Wire-Four Leg Shunt Active Filter for Harmonic and Reactive Power Compensation. *Energy and Power Engineering*, 3, 422-435.

Ravindra, G. M., Gopi, S. P. & Kalavathi, M. S. (2012). Power Quality Improvement in Deregulated Power System by Using Active Filters. *International Journal of Scientific & Engineering Research,* 3(6), 1-5.

Renu, S., Deepak, K. G., Harpreet, S. (2016). Analysis of Space Vector PWM for Three Phase Inverter and Comparison with SPWM. *International Journal of Advanced Research in Electrical, Electronics and Instrumentation Engineering,* 5(1), 533-540.

Roger, C. D., Mark, F. M., Surya, S. & Wayne, H. B. (2004). Electrical Power Systems Quality *Second edition. McGraw-Hill, New York.*

Sankara. C. (2002). Power quality. *CRC Press, New York.*

Saravana, P. & Balachrishnan, P. A. (2014). An Efficient Space Vector Modulation (SVPWM) with BFO Based Self-Tuning PI Controller for Shunt Active Power Filter (SAPF). *Research Journal for Applied Sciences, Engineering and Technology*, 7(20), 4281-4295.

Shafiuzzaman, K. K. (2013). Power Quality Improvement of Distributed Generation Integrated Network with Unified Power Quality Conditioner. *PhD. Thesis, Electrical Engineering Systems, Dublin Institute of Technology, Republic of Ireland.*

Shafiuzzaman, K. K., Basu, M. & Conlon, M. F. (2014). Harmonic Power Compensation Capacity of Shunt APF and its Relationship to Design Parameters. *IET Power Electronics,* 7(2), 418 – 430.

Shrutisnata, M. (2016). Power Quality Improvement Using Unified Power Quality Conditioner. *M.Sc. Thesis, Department of Electrical Engineering, National Institute of Technology, Rourkela.*

Shashibhushan R. S. & Nikhil A. W. (2017). Performance Analysis of Shunt Active Power Filter with Various Switching Signal Generation Techniques. International Journal of Engineering Development and Research. 5(2),2321-9939.

Sindhu, M. R., Manjula, G. N. & Nambiar, T.N. (2015). Three-Phase Tuned Shunt Hybrid Filter for Harmonic and Reactive Power Compensation. *Elservier Procedia Technology* 21, 482-489.

Soomro, D. M., Omran, M. A. & Alswed, S. K. (2015). Design of Shunt Active Power Filter (SAPF) to Mitigate the Harmonics Caused by Non-Linear Loads. *APPN Journal of Engineering and Applied Sciences,*10(19), 8774-8782.

Subhransu, S. & Siddharth, S. B. (2016). Theory Modulation Space Vector. *Vietnan Journal of Science Technology and Engineering*, YouTube.

Suleiman, M., Mohd, A. M., Hashim, H., Noor, I. A., Yap, H. & Mohammad, A. A. (2017). Modified Synchronous Reference Frame (SRF) Based Shunt Active Power Filter (SAPF) With Fuzzy Logic Pulse Width Modulation (FLC-PWM) Inverter. *Energies 2017 Journal*, 10(785), 1-17.

Sunitha, M., & Kartheck, B. N. (2013). Elimination of Harmonics Using Shunt Active Power Filter (SAPF) Based on D-Q Reference Frame Theory. *International Journal of Engineering Trends and Technology (IJETT)*, 4(4), 781-785.

Suresh, M. & Anup, K. P. (2011). Id-Iq Control Strategies for Mitigation of Current Harmonics with Fuzzy Logic Controller using Matlab/Simulation and RTDS Hardware. *Intelligent Control and Automation*, 2, 371-382.

Tej, K. R. & Ruchi, P. (2014). *Space Vector Modulation and Maximum Power Tracking Control on Photovoltaic Power Generation System.* Paper presented at 11th IRF International Conference, Pone, India, 59-63.

Thamizhazhagan, P & Sutha, S (2015). Analysis of PWM Techniques for Power Quality Improvement in PMSM Drives. *Indian Journal of Science and Technology*, 8(24), 1-5.

Umar, B.M. (2017). Modeling and Simulation of Compact Fluorescent Lamp for the Analysis and Mitigation of Harmonics Injection into Power Distribution Network. *M.Sc Thesis, Department of Electrical and Computer Engineering, Ahmadu Bello University, Zaria, Nigerian.*

Varaprasad, O. & Siva, D.V. (2014). An Improved SVPWM Based Shunt Active Power Filter (SAPF) for Compensation of Power Harmonics. *IEEE Transacts*, 571-575.

Venkata, B. S., Mahesh, B. B., Ravi, L. S. & Tulasiram, S. S. (2014). Design of Shunt Active Power Filter (SAPF) for Improvement of Power Quality with Artificial Intelligence Techniques. *International Journal of Advance Research in Electrical, Electronics and Instrumentation Engineering*, 3(8), 11304-11314.

Yogesh, D. (2011). Power Quality Improvement by Employing PWM Techniques and Fuzzy Logic Based Shunt Power Filter (SAPF). *M.Sc Thesis, Thapar University, Patiala 147004, Punjab, Indian.*

Zahira, R. & Peer, A. F. (2012). Technical Survey on Control Strategies of Shunt Active Power Filter (SAPF) for Harmonics Suppression. *Elsevier Procedia Engineering* (30), 686-693.

APPENDIX A

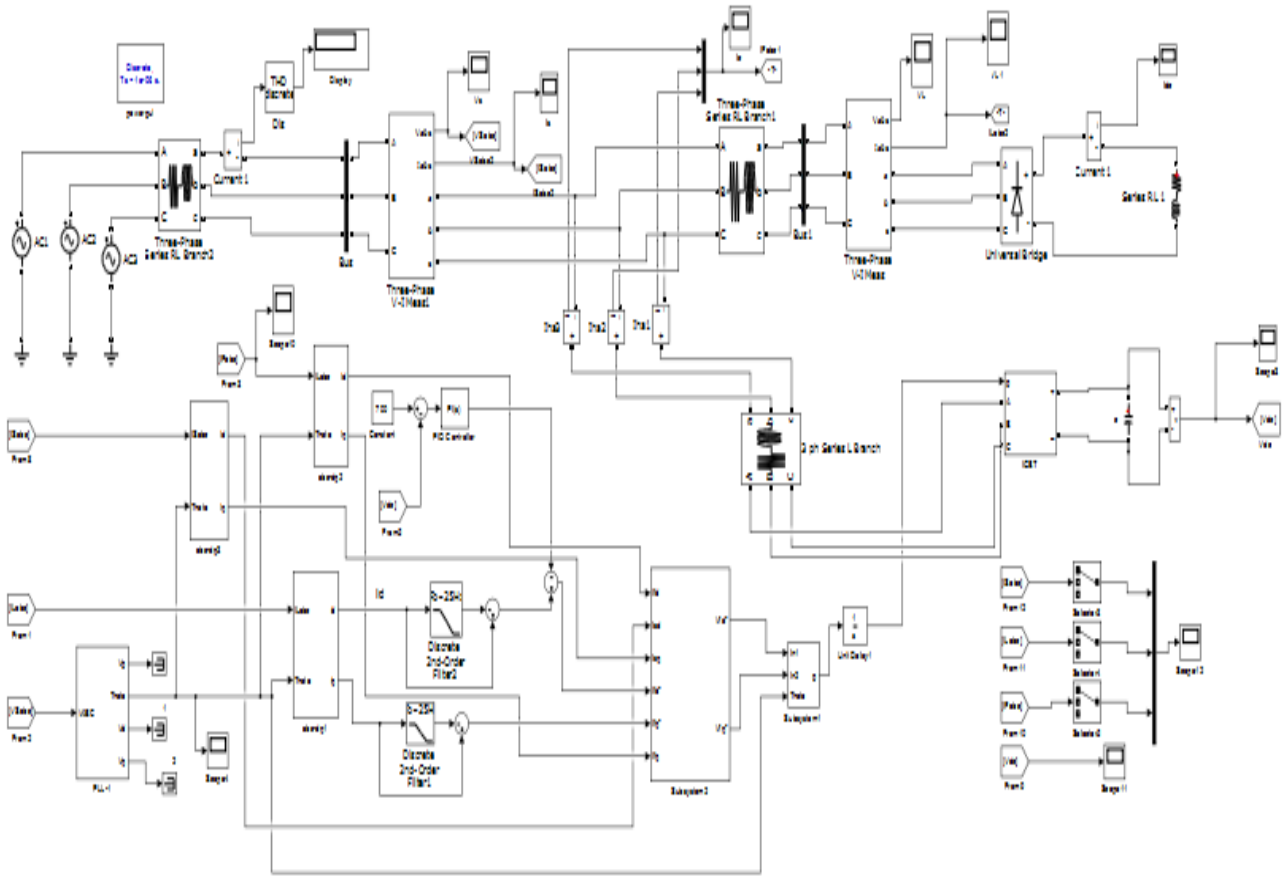


Figure A1: Complete Simulink Models of SAPF

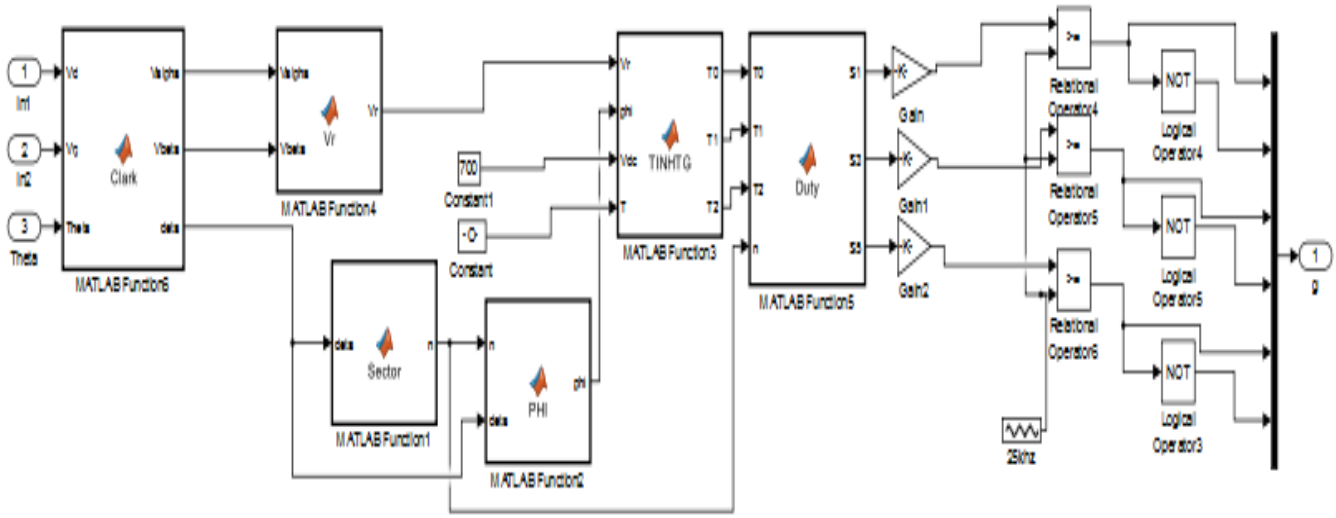


Figure A2: Complete Simulink Models of SVPWM